Fayalite oxidation processes in Obsidian Cliffs rhyolite flow, Oregon

(Revision 1)

Audrey M. Martin [1,2], Etienne Médard [3,4,5], Bertrand Devouard [6], Lindsay P. Keller [1], Kevin Righter[1], Jean-Luc Devidal [3,4,5] and Zia Rahman[1]

[1] NASA Johnson Space Center, Mailcode KT, 2101 NASA Parkway, Houston, TX 77058 USA

[2] Earth, Environmental and Planetary Sciences, Case Western Reserve University, 10900 Euclid Avenue, Cleveland, OH 44118 USA

[3] Clermont Université, Université Blaise Pascal, Laboratoire Magmas et Volcans, BP 10448, F-63000 Clermont-Ferrand, France

[4] CNRS, UMR 6524, LMV, F-63038 Clermont-Ferrand, France

[5] IRD, R 163, LMV, F-63038 Clermont-Ferrand, France

[6] CEREGE, Europôle Méditerranéen de l'Arbois, Avenue Louis Philibert, BP 80, F-13545 Aix-en-Provence, France

ABSTRACT

This study investigates the oxidation of *fayalite* $Fe^{2+}_2SiO_4$ that is present in lithophysae from a rhyolite flow (Obsidian Cliffs, Oregon, USA). Textural, chemical and structural analyses of the successive oxidation zones are used to constrain (1) the oxidation processes of olivine and (2) the role of temperature, chemical diffusion and meteoric infiltration. Petrologic analyses and thermodynamic modeling show that the rhyolite flow emplaced at 800-950°C. *Fayalite*-bearing lithophysae formed only in the core of the lava flow. Variations in the gas composition inside the lithophysae induced the oxidation of *fayalite* to a *laihunite* zone $Fe^{2+}Fe^{3+}_2\square(SiO_4)_2$. This zone is made of nano-lamellae of amorphous *silica* SiO_2 and *laihunite* + *hematite* Fe_2O_3. It probably formed by a nucleation and growth process in the *fayalite* fractures and defects and at *fayalite* crystal edges. The *laihunite* zone then oxidized into an "*oxyfayalite*" zone with the composition $Fe^{2+}_{0.26}Fe^{3+}_{1.16}\square_{0.58}SiO_4$. This second oxidation zone is made of lamellae of amorphous *silica* and *hematite* Fe_2O_3, with a possible small amount of *ferrosilite* $Fe^{2+}SiO_3$. A third and outer zone, composed exclusively of *hematite*, is also present. The successive oxidation zones suggest that there may be a mineral in the olivine group with higher Fe^{3+} content than laihunite. The laihunite transformation to this "*oxyfayalite*" could occur by a reaction such as:

$$0.24\ Fe^{2+}_{M1}{}^{\text{laihunite}} + 0.06\ O_2 = 0.16\ Fe^{3+}_{M1}{}^{\text{"oxyfayalite"}} + 0.08\ \square^{\text{"oxyfayalite"}} + 0.04\ Fe^{3+}_2O_3{}^{\text{hematite}}$$

This would imply that Fe^{3+} can also be incorporated in the M1 site of olivine.

KEYWORDS

Olivine, fayalite, laihunite, "oxyfayalite", rhyolite, lithophysae, oxidation

INTRODUCTION

Olivine is one of the most important minerals in planetary sciences. It crystallizes in the orthorhombic system (space group Pbmn) and forms a solid solution between two end-members, *forsterite* Mg_2SiO_4 and *fayalite* Fe_2SiO_4. *Forsterite*-rich compositions are the most frequent; however, the f*ayalite* end-member (cell parameters a = 4.818 Å, b = 10.471 Å, c = 6.086 Å at 1 atm. and 20°C; Smyth 1975) has been observed in some terrestrial rocks and primitive meteorites (CV3 chondrites; Hua and Buseck 1995; Jogo et al. 2009). Iron oxidation in contact with the atmosphere / hydrosphere is known to induce *olivine* destabilization. *Hematite* Fe_2O_3 (trigonal, R-3c, a = 5.038 Å, c = 13.772 Å; Blake et al. 1966) and *magnetite* Fe_3O_4 (isometric, Fd3m, a = 8.397 Å) precipitates were found in natural oxidized *olivines* from the Sulu peridotite (Hwang et al. 2008). Using experiments, Champness (1970) described a low temperature (500 - 800°C) *olivine* oxidation process in air by the nucleation and growth of amorphous *silica* SiO_2 and *magnetite* or *hematite*. Wu and Kohlsted (1988) obtained similar oxidation of *olivine* (Fa_{10}) to *magnetite* plus amorphous *silica* in experiments heated between 700 and 1100°C during 0.5 to 100 hours. Khisina et al. (1995), however, observed the formation of *ferriforsterite* $Mg_{0.5}\square_{0.5}(Fe^{3+})_{1.0}SiO_4$, *magnesioferrite* $MgFe_2O_4$ and *magnetite* from the oxidation of *olivine* (Fa_{11}) at temperatures between 350 and 700°C after 48 to 70 hours.

A Mg-free ferric *fayalite*, *laihunite* $Fe^{2+}Fe^{3+}_2\square(SiO_4)_2$, has also been reported in Earth samples (magnetite ore, metamorphic and volcanic rocks; mafic xenoliths; *Laihunite* Research Group, 1976, 1982; Shengyuan 1982; Schaefer 1983a,b, 1985; Tamada 1983; Kitamura et al. 1984; Sueno et al. 1985; Dyar et al. 1998; Faure et al. 2001) and in Martian meteorites (nakhlites; Noguchi et al. 2009; Kuebler 2013). It has been synthesized at 1 atmosphere between

400 and 700°C (Kondoh et al. 1985; Khisina et al. 1998; Tomioka et al. 2012). Mg-free *laihunite* is believed to form by oxidation reactions such as:

$$6\ Fe^{2+}_2\ SiO_4 + 2\ O_2 = 3\ Fe^{2+}_1Fe^{3+}_2\square_1(SiO_4)_2 + Fe_3O_4 \qquad (1)$$

6 fayalite + 2 O_2 = 3 laihunite + magnetite

or

$$8\ Fe^{2+}_2SiO_4 + 3\ O_2 = 4\ Fe^{2+}_1Fe^{3+}_2\square_1(SiO_4)_2 + 2\ Fe_2O_3 \qquad (2)$$

8 fayalite + 3 O_2 = 4 laihunite + 2 hematite

Fe^{3+} is incorporated in the *laihunite* structure through the heterovalent substitution 3 Fe^{2+} = 2 Fe^{3+} + □. It has been suggested that Fe^{3+} can only be incorporated in the slightly larger M2 site, leading to the *laihunite* end-member $^{M1}(Fe^{2+}\square)^{M2}Fe^{3+}_2(SiO_4)_2$. Several polytypes of laihunite have been described, with different Fe^{3+}/Fe_{tot} ratio and structure:

- *laihunite-1M* $Fe^{2+}_1Fe^{3+}_2\square_1(SiO_4)_2$. According to Fu et al. (1982) and Xu et al. (2014), it is the most Fe^{3+}-rich *laihunite* polytype. It has a distorted olivine structure (space group $P2_1/b$) with a monoclinic crystal symmetry and cell parameters a = 4.80 ± 0.02 Å, b = 10.20 ± 0.02 Å, c = 1*5.80 ± 0.02 Å and α = 91.39° (Xu et al. 2014).

- *laihunite-2M* also has a monoclinic symmetry ($P2_1/b$), but with a two-layer superstructure that accommodates the Fe^{3+} cations present in the mineral structure (Pingqiu et al. 1982; Kondoh et al. 1985; Shen et al. 1986). According to Kondoh et al. (1985), *laihunite-2M* composition is $Fe^{2+}_{0.90}Fe^{3+}_{0.73}\square_{0.37}(SiO_4)_2$. However, Xu et al. (2014) re-evaluated it to $Fe^{2+}_{2.5}Fe^{3+}_1\square_{0.5}(SiO_4)_2$. According to Xu et al., its cell parameters are a = 4.82 ± 0.02 Å, b = 10.30 ± 0.02 Å, c = 2*5.93 ± 0.02 Å and α = 90.79°.

- the third polytype is characterized by three-layer superstructures along the c axis. It has been described either as *laihunite-3M* or *laihunite-3Or*. L*aihunite-3M* has a composition $Fe^{2+}_{1.6}Fe^{3+}_{1.6}\square_{0.8}SiO_4$ and a monoclinic crystal symmetry (P 2_1/b) and cell parameters a = 4.805 Å, b = 10.189 Å, c = 17.403 Å and α = 91.0° (Shen et al. 1986). Laihunite-3Or has a Pbmn structure and a structural formula $Fe^{2+}_3Fe^{3+}_2\square(SiO_4)_3$ (Xu et al. 2014). According to Xu et al. experimental results, its cell parameters are a = 4.81 ± 0.02 Å, b = 10.25 ± 0.02 Å, c = 3*5.85 ± 0.02 Å and α = 90.0°.

Previous studies suggest that no solid solution exists between *fayalite* and *laihunite-1M* at ambient temperature and pressure. Detailed SEM, Mössbauer and TEM studies indicate that *laihunite-2M* and *laihunite-3M* can be considered as intergrowths of the pure end-members *fayalite* and *laihunite* at the nano-scale (Schaefer 1985, Xu et al. 2014).

The existence of the *laihunite* polytypes suggests that phases with higher Fe^{3+} - between *laihunite-1M* and the theoretical pure end-member "*ferrifayalite*" $Fe^{3+}_4\square_2(SiO_4)_3$ - might also be stable, but not yet discovered. Their existence would, however, require that Fe^{3+} could be incorporated in the M1 site, or that the M1 and M2 sites become equivalent at high temperature. The structure of an oxidized *fayalite* with a Fe^{3+} fraction higher than *laihunite* would also certainly be modified by the presence of magnesium or manganese (Janney and Banfield 1998), if it can incorporate this element in its structure.

Other minerals may also form during *fayalite* oxidation. *Pyroxene* like *ferrosilite* $FeSiO_3$ (orthorhombic, Pbca, a = 18.527 Å; b = 9.145 Å; c = 5.2756 Å at 600°C; Sueno et al. 1976) has been reported by Gualtieri et al. (2003). According to Khisina et al. (2000), the oxidation of *fayalite* at 700°C in air may also produce hydrous minerals such as *feroxyhyte* δ-$Fe^{3+}O(OH)$

(hexagonal, P-3m1, a = 2.95 Å; c = 4.56 Å) and *bernalite* $Fe^{3+}(OH)_3$(orthorhombic, Immn, a = 7.544 Å, b = 7.560 Å, c = 7.558 Å). *Goethite* α-$Fe^{3+}O(OH)$ (orthorhombic, Pnma, a = 4.608 Å; b = 9.956 Å; c = 3.0215 Å), *lepidocrocite* □-$Fe^{3+}O(OH)$ (orthorhombic, Cmc2, a = 3.88 Å; b = 12.54 Å; c = 3.07 Å), *ferrihydrite* $Fe^{3+}{}_5O_3(OH)_9$ (hexagonal, P-31c, a = 2.96 Å; c = 9.4 Å) and *iron hydroxide* $Fe(OH)_2$ (P-3m1; a = 3.262; c = 4.596) may also form.

In the following, we present data from naturally oxidized *fayalite* that strongly hints at the existence of a phase that is more oxidized than *laihunite* and close to the *"ferrifayalite"* end-member $Fe^{3+}{}_4□_2(SiO_4)_3$. These *fayalite* crystals were sampled in the talus of the Obsidian Cliffs rhyolite flow, East of McKenzie Pass in the Oregon Cascades, USA (Fig.1a). The upper part of the flow is mostly a compact and glassy obsidian with spherulites, containing deformed microlite flow banding (Fig.1b); the lower part is a light gray to pink rhyolite. The lightest gray rhyolite zones contain large (up to 10 mm) and cavernous lithophysae (Fig.1c). During cooling of the lava flow, various minerals grew on the walls of the gas-filled vugs, towards the center. Obsidian Cliffs' lithophysae contain well-formed crystals of *fayalite* Fe_2SiO_4, *tridymite* SiO_2, *phlogopite* $KMg_3(AlSi_3O_{10})(OH,F)_2$ and *osumilite* $(K_{0.65},Na_{0.08},Ca_{0.02})_{0.75}(Fe^{2+}{}_{0.98},Mg_{0.88},Mn_{0.11})_{2.00}(Al_{2.75},Fe^{3+}{}_{0.19})_{2.94}(Si_{10.41},Al_{1.59})_{12}O_{30}$ (Olsen and Bunch 1970) (Supplementary Material 1). *Fayalite* and *mica* crystals are covered with a layer of rusty to iridescent oxidation products (Fig.1d&e). A selected *fayalite* crystal from Obsidian Cliffs' gray rhyolite was mounted in epoxy and sliced (Fig.2a&b) in order to (1) investigate fayalite oxidation mechanisms and (2) constrain the role of temperature, chemical diffusion and meteoric infiltration. We constrained the composition, iron oxidation state and structure of

each oxidation zone and compared them to the previous studies on natural and experimental samples of oxidized olivine.

ANALYTICAL TECHNIQUES

SEM/EMPA imaging and analysis

Large-scale back scattered electron (BSE) images of the sample sections were obtained on an electron microscope (Cameca SX100; LMV) (Fig.2). Chemical analyses of the various *fayalite* zones and of the *osumilite* were made by wavelength dispersive X-ray spectroscopy using the same EMPA, with an accelerating voltage of 15 kV and a beam current of 15 nA (Supplementary Material 2). H*ematite* could not be analyzed due to its small size. The standards used were *fayalite* Fe_2SiO_4 for Fe, *forsterite* Mg_2SiO_4 for Mg, *wollastonite* $CaSiO_3$ for Ca and Si, and *manganese titanate* $MnTiO_3$ (synthetic) for Mn. EMPA was also used for the quantitative determination of $Fe^{3+}/\sum Fe$ in the various zones using the Fe*Lα* peak shift (Fialin et al. 2001, 2004). The analytical conditions were fixed at 15 kV and 100 nA. The Fe^{2+} and Fe^{3+} calibration curves were determined using silicates (*olivine*, *garnet, pyroxene* and *epidote*) and oxides (*hematite*) as standards (Supplementary Material 3). Seven to eight analyses were made on each standard. OriginPro8© software was used for the data treatment. A logarithmic curve was used for Fe^{2+} calibration data fitting, while a linear curve was chosen for Fe^{3+} as in Fialin et al. (2004).

TEM imaging and analysis

A thin slice was prepared in one of the *fayalite* crystals using focused-ion beam (Quanta 3D FEG; ARES/JSC). The slice was oriented in the (010) direction of the crystal, and its length was fixed in order to include *fayalite* and the *laihunite* and "*oxyfayalite*" oxidation zones (Fig.2b).

Analyses were run with a field-emission scanning transmission electron microscope (JEOL 2500 SE; ARES/JSC) in order to determine: (1) the nano-texture of the various zones, (2) the structure of the phases and (3) the $Fe^{3+}/\sum Fe$ ratio in the phases. Selected area electron diffraction (SAED) pattern were modeled using SingleCrystal©/CrystalMaker2.1© software. Ferric iron fraction was determined using Electron Energy Loss Spectroscopy (Gatan 666 PEELS) (Gloter et al. 2000; van Aken and Liebscher 2002). EELS spectra were processed using OriginPro7.5© software with Lorentzian function.

RESULTS

Phase relations and micro-textures in the lithophysae

Obsidian Cliffs' lithophysae contain *fayalite*, *osumilite*, *phlogopite*, *tridymite* and *hematite*. Relatively similar mineralization has been found in lithophysae from Monte Arci, Sardinia, Italy and Henderson Quarry, Ngongotaha Dome, New Zealand (Supplementary Material 1).

Fayalite

Obsidian Cliffs' *fayalite* crystals are covered with oxidation products (Fig.2a&b). Numerous oxidized zones are also observed within the crystals. Using their shape, they can be classified into two types of objects: well-zoned objects – which are either elongated (often with a spindle shape) or rectangular – and complex dendritic objects.

Well-zoned objects are organized around a small bright core (*hematite*) that has sometimes a hole in its center. Two zones with intermediate contrast are observed around these bright cores, in addition to *fayalite* (Fig.2b; see 3.2.1.). The separation between the different zones is extremely sharp in reflected light images as well as in BSE images. Elongated

objects are oriented either in the (010) direction of the *fayalite* crystal or between 30 and 50° of this direction. Rectangular objects are often aligned with the elongated objects and might represent different sections of the same spindle shaped objects.

Dendritic objects have poorly defined internal structures that certainly indicate complex growth process. They grew perpendicularly to fractures, in the same directions as the well-zoned elongated objects.

Osumilite

Osumilite is also present in Obsidian Cliffs' lithophysae, as observed by Olsen and Bunch (1970). It forms large euhedral crystals of up to 1 mm (Fig.2c). These crystals contain some inclusions of *silica* that probably served as nuclei for *osumilite* crystallization.

Phlogopite

As described by Olsen and Bunch (1970), *mica* crystals are oxidized to *hematite* in our samples. *Mica* "ghosts" are mostly euhedral and up to 400 µm long (Fig.2d). Bulk qualitative analysis of a mica pseudomorph is close to phlogopite composition with small amount of iron. However, since no fresh mica is available, the initial composition (before oxidation) could have been that of a *phlogopite*, a *fluorophlogopite*, or an *oxyphlogopite*.

Tridymite

Silica crystals of less than 100 µm are present all around the walls of the lithophysae (Fig.2c&d). We cannot distinguish *quartz* and *tridymite* using electron microprobe; however, the elongated crystal sections are indicative of *tridymite* rather than *quartz*. This is concordant with the observation of Olsen and Bunch (1970) who found that *tridymite* is present in the lithophysae of their Obsidian Cliffs' rhyolite samples.

Phase compositions

Fayalite

The non-oxidized portions that comprise the bulk of the crystals have a stoichiometric *fayalite* composition, with a significant MgO (7 ± 2 wt%) and MnO (5 ± 1 wt%) contents; Fig.3; Supplementary Material 2). The oxidized portions cluster around three compositions:

(1) a composition with the stoichiometry of *laihunite* $Fe^{2+}Fe^{3+}{}_2\square(SiO_4)_2$ that corresponds to the bulk of the dendritic objects as well as the external part of the well-zoned objects. This zone has much lower MnO (0.45 ± 0.05 wt%) and MgO (0.14 ± 0.05 wt%) contents.

(2) a composition more depleted in iron, plotting near the theoretical "*ferrifayalite"* end-member $Fe^{3+}{}_4\square_2(SiO_4)_3$ that is measured in the central part of the well-zoned objects (around the bright *hematite* core). The MnO and MgO contents of this zone are very low (0.27 ± 0.09 and 0.06 ± 0.03, respectively). As it also contains a small amount of Fe^{2+} (see 3.4.), it will be called "*oxyfayalite*" rather than "*ferrifayalite*" in the following.

(3) *hematite* $Fe^{3+}{}_2O_3$ that we could not analyze due to its small size.

No intermediate composition between *fayalite* and *laihunite* is observed, contrary to the samples investigated by Schaefer (1985). Chemical continuity between well-zoned objects and the external part of dendritic objects is sometimes visible on BSE images. In the following, we will therefore distinguish the preserved *fayalite* zone and three oxidation zones named according to their bulk composition: the "*laihunite*" zone, the "*oxyfayalite*" zone and the "*hematite*" zone.

Osumilite

The composition of Obsidian Cliffs' *osumilite* (Supplementary Material 2) is very similar to that determined by Olsen and Bunch (1970), with a slightly higher $Fe^{3+}/\Sigma Fe = 0.25 \pm 0.62$ (compared to 0.16) and an atomic formula $(K_{0.71},Na_{0.01},Ca_{0.01})_{0.75}(Fe^{2+}_{1.01},Mg_{0.85},Mn_{0.15})_{2.00}(Al_{2.67},Fe^{3+}_{0.33})_{2.94}(Si_{10.32},Al_{1.68})_{12}O_{30}$. This Fe-rich osumilite has approximately the same composition as the osumilite from Monte Arci, Sardinia (Olsen and Bunch 1970, Elmi et al 2010). Obsidian Cliffs' and Monte Arci's osumilites are, however, more iron-rich (Mg# = $Mg/(Mg+Fe_{tot}+Mn)$ = 0.36 ± 0.03 and 0.33 ± 0.1, respectively) than the osumilite found in the lithophysae from the Ngongotaha Dome, New Zealand (Mg# = 0.62, Grapes et al. 1993), that rather falls within the Mg-osumilites domain.

Nano-texture and structure of the fayalite oxidation zones

The images obtained by transmission electron microscope on a well-zoned object in the fayalite crystal are shown in Figure 4, and the corresponding diffraction patterns in Figure 5. The *fayalite* zone has a homogeneous nano-texture and structure (Fig. 4a, 4b and 4c), with parameters corresponding to theoretical *fayalite* $Fe^{2+}_2SiO_4$ (Fig. 5a and 5d). On contrary, the nano-texture of the *laihunite* and "*oxyfayalite*" zones is heterogeneous. Both zones are composed of alternate dark and white "lamellae".

***Laihunite* zone**

The *laihunite* zone is composed of white lamellae of amorphous *silica* SiO_2 and dark lamellae of iron- and silicon-rich material (Fig. 4c, 4d and 4e). The diffraction pattern of the dark lamellae (Fig. 5b) shows that they are composed of two phases (Fig.5e):

(1) a phase that has superstructures along the c axis similar to *laihunite*, with lattice parameters close to the *laihunite-3M* defined by Shen et al. (1986);

(2) *hematite* $Fe^{3+}_2O_3$ that increases the whole Fe^{3+} fraction in the *laihunite* zone (explaining why its composition is closer to that of *laihunite-1M)*.

"*Oxyfayalite*" zone

Like the "*laihunite*" zone, the "*oxyfayalite*" zone is composed of dark and white lamellae (Fig. 4e and 4f). The white lamellae are made of amorphous *silica*. SAED pattern of the dark lamellae (Fig. 5c) is concordant with *hematite* (Fig. 5f). The diffuse and elongated appearance of the *hematite* diffraction spots reflects the lamellae structure. A decomposition of the theoretical pure Fe^{3+} *fayalite* end-member to *silica* and *hematite* could occur by the reaction:

$$Fe^{3+}_4□_2(SiO_4)_3 = 3\ SiO_2 + 2\ Fe^{3+}_2O_3 \quad (4)$$

oxyfayalite = 3 amorphous silica + 2 hematite

The resulting *silica*/oxide molar ratio should be around 1.5, and the volume fractions of approx. 63 vol.% for *silica* and 37 vol.% for *hematite*. Phase proportions estimated from TEM images, however, give a volume fraction of amorphous *silica* around 51 ± 5 vol.%, and a volume fraction of dark lamellae around 49 ± 5 vol.%. Quantitative microprobe analyses also suggest the presence of a Fe^{2+}-bearing phase in the dark lamellae, which is confirmed by the iron oxidation state measurements (see 3.4.). Some Fe^{2+} could be present in the *hematite* structure. However, another phase like *ferrosilite* $Fe^{2+}SiO_3$ might also be portrayed by the SAED pattern of dark lamellae (in addition to *hematite*) and could explain the presence of ferrous iron (Fig.5f).

Interfaces

Remarkable structural relationship is observable at the interface between the *fayalite* and *laihunite* zones (Fig. 4a, 4b and 4c). The whole *fayalite – laihunite* boundary is marked by crenels of approx. 10 nm width and 10 to 20 nm length, corresponding to the extremity of the

laihunite zone lamellae (Fig. 4c). Dark lamellae extend farther into *fayalite* than white lamellae. SAED patterns made on those crenels show a combination of the diffraction patterns of the fayalite and laihunite zones. Some fractures are also present in the *fayalite* zone, perpendicularly to the interface. These fractures are filled with lamellae similar in composition to those present in the *laihunite* zone. However, they have particular orientation that makes them resemble "feathers" extending far into the *laihunite* zone (Fig. 4a and 4b).

The interface between the *laihunite* and the "*oxyfayalite*" zones is less organized (Fig. 4e). It is marked by a long "fracture" filled mostly with amorphous material and some rounded parts of unidentified dark material that could be remnants of dark lamellae from either or both of the two oxidation zones. This interface resembles a resorption feature.

Iron oxidation state

$Fe^{3+}/\sum Fe$ was measured within each zone using the position of the $Fe_{L\alpha}$ peak on the electron microprobe (Fig. 6a; Supplementary Material 3) and using Electron Energy Loss Spectroscopy on TEM (Fig. 6b; Supplementary Material 4). The iron oxidation state measured by microprobe evolves from the reduced *fayalite* parts of the crystal, to more oxidized zones, i.e., the *laihunite* zone, the "*oxyfayalite*" zone and finally the *hematite* zone. In the *fayalite* zone, $Fe^{3+}/\sum Fe$ is near zero according to both microprobe and EELS data. Fe^{3+} fraction in the *laihunite* zone is 0.61 ± 0.03 using EELS and around 0.65 ± 0.06 using microprobe, which is near the theoretical value of 0.66 for *laihunite* $Fe^{2+}Fe^{3+}{}_2\square(SiO_4)_2$. Fe^{3+} fraction in the "*oxyfayalite*" zone is 0.82 ± 0.06 according to EELS results and around 0.8 ± 0.1 using microprobe, i.e., a lower value than the one expected for the theoretical pure *ferrifayalite* end-member. Considering this observed value and the charge balance constraints (that give a theoretical formula $Fe^{2+}{}_{2-}$

278 $_{3x}Fe^{3+}{}_{2x}\square_xSiO_4$; Kondoh et al. 1985), the whole "*oxyfayalite*" zone has a structural formula
279 $Fe^{2+}{}_{0.26}Fe^{3+}{}_{1.16}\square_{0.58}SiO_4$.

280 **DISCUSSION**

281 **Formation and crystallization of the lithophysae**

282 Several hypotheses have been evoked to explain the formation of lithophysae, in
283 particular, with regard to spherulites formation (Lofgren 1971a, 1971b; Breitkreuz 2013). The
284 presence of the lithophysae cavities is mostly explained in two ways: (1) the contraction of the
285 lava during cooling creates voids where fluids migrate, or (2) the exsolution of volcanic fluids
286 creates "bubbles" in the lava flow (Breitkreuz 2013).

287 Considering its texture and relationship with the other minerals, *tridymite* was probably
288 one of the first phases to crystallize inside the lithophysae. *Fayalite* then crystallized, followed
289 by (or simultaneous with) *osumilite*. *Phlogopite* probably formed by the destabilization of
290 osumilite during the temperature decrease, as suggested by Olsen and Bunch (1970). *Hematite*
291 is also a secondary mineral, which formed by the oxidation of iron during the lava flow cooling
292 (see below).

293 **Oxidation process of fayalite**

294 **Chemical process**

295 Considering our analyses, the oxidation reaction that lead to the formation of the
296 *laihunite* zone can be written:

297 $$3\ Fe_2SiO_4 + 1\ O_2 = 1\ SiO_2 + 1\ Fe^{2+}Fe^{3+}{}_2\square(SiO_4)_2 + 1\ Fe^{2+}Fe^{3+}{}_2O_4 \qquad (5)$$

298 3 fayalite + 1 vapor = 1 amorphous SiO_2 + 1 laihunite + 1 magnetite

299 In theory, "*oxyfayalite*" can form by a reaction such as:

$$12\ Fe^{2+}\square Fe^{3+}_2(SiO_4)_2 + 3\ O_2 = 8\ Fe^{3+}_4\square_2(SiO_4)_3 + 2\ Fe^{3+}_2O_3 \qquad (6)$$

12 laihunite + 3 O_2 = 8 “oxyfayalite” + 2 hematite

with hematite moving to the outer oxidation layer. In our case, the “oxyfayalite” phase is not homogeneous, but made of nano-lamellae of amorphous *silica* and *hematite*. Either an *oxyfayalite* phase formed by reaction (6) and later broke down to *hematite* and *silica*, or reaction (6) should rather be written:

$$4\ Fe^{2+}\square Fe^{3+}_2(SiO_4)_2 + O_2 = 8\ SiO_2 + 6\ Fe^{3+}_2O_3 \qquad (7)$$

4 laihunite + O_2 = 8 amorphous silica + 6 hematite

with part of the hematite moving to the outside. Note that this reaction does not take into account the small amount of Fe^{2+} ($Fe^{2+}/(Fe^{3+}+Fe^{2+})$=0.18) in the “oxyfayalite” zone, which could be present either in the hematite structure or in an additional phase like ferrosilite.

Considering the nature of the interface between the two oxidation layers – a long “fracture” filled with amorphous material – and the absence of any crosscutting feature, these two oxidation stages certainly occurred successively rather than simultaneously, in reaction to variations in external parameters. Their formation, however, may have occurred within a short duration (see below).

The oxidation of Obsidian Cliffs’ fayalite was also accompanied by chemical diffusion. As suggested by Wu and Kohlsted (1988) and Ashworth and Chambers (2000), Si^{4+} and O^{2-} probably stayed immobile, while iron migrated to the more oxidized zones. Microprobe analyses also show that the higher the Fe^{3+} fraction in the “*fayalite*” structure, the lower the Mg and Mn contents. However, Mg- and Mn-bearing forms of *laihunite*, *magnetite* and *hematite* were reported in natural samples (Shen et al. 1986; Noguchi et al. 2009). This absence can rather be

322 explained by contrasting elemental diffusion rates. According to Wu and Kohlsted (1988) and
323 Khisina et al. (1995, 2000), Mg diffuses faster than Fe during *fayalite* oxidation, leading to Mg-
324 free inner oxidation zones, and Mg-rich outer oxidation zones. Similarly, no magnesium is
325 observed in the outer oxidation layer of our sample (though hematite could not be analyzed).
326 This Mg may have participated in the formation of phlogopite, as the magnesium from osumilite
327 (Olsen and Bunch, 1970). Before that, it should have dissolved into the fluids. Mg^{2+} may have
328 dissolved more or less depending on the fractions of H, O, C, and S during fayalite oxidation.
329 Numerous studies have been conducted on the solubility of magnesium from olivine in aqueous
330 environments. In particular, Chen and Brantley (2000) determined that olivine releases Mg and
331 Si more rapidly than Fe at 65°C and pH 5, probably because of the simultaneous oxidation of the
332 mineral surface. Further study should be performed to determine the solubility of magnesium in
333 H-O-C-S fluids from fayalite dissolution at high temperature (600-800°C) to confirm the transfer
334 of Mg from fayalite to osumilite if other volatile species like C and S are presence in the gas,

335 The absence of manganese in the *laihunite* and "*oxyfayalite*" zones indicates that it also
336 probably diffused faster than iron during *fayalite* oxidation. Thermodynamic calculations (Fig.7)
337 show that Mn^{2+} should oxidize to Mn^{3+} at approximately the same temperature – fO_2 conditions
338 as the *hematite* – *magnetite* buffer. *Hausmannite* Mn_3O_4 and *bixbyite* Mn_2O_3 have been
339 observed in rhyolites from Western United States (Fries et al. 1942, Burt et al. 1982,
340 Christiansen et al. 1983), but they have never been found in Obsidian Cliffs rhyolite. Mn^{3+} could
341 also be incorporated into the outer *hematite*. However, Mn^{3+} is stable in the *hematite* structure
342 at high temperature only. According to Muan and Somiya (1961), *hematite* with more than ~6
343 wt% Mn_2O_3 forms *bixbyite* (Mn_2O_3) + *hematite* (Fe_2O_3) below 700°C at 1 atmosphere. Therefore,

the manganese content in hematite may be very low. Like magnesium, manganese may have dissolved as cations (Mn^{2+}, Mn^{3+}) into the fluid and been incorporated by osumilite.

Textural evolution

The *fayalite* crystals sampled at Obsidian Cliffs exhibits surficial as well as interior oxidation. Interior oxidation probably occurred by fluid migration within fractures or defects. Oxidation phases developed with *fayalite* morphology (Fig. 8).

The lamellar nano-texture observed in the *laihunite* and "*oxyfayalite*" zones could be attributed to two processes:

(1) it may have formed by late exsolution occurring at the end of the temperature decrease (Ashworth and Chambers 2000). This hypothesis would imply that crystalline *laihunite* and *oxyfayalite* phases have been temporarily stable at high temperature conditions. In this case, a destabilization reaction of the *oxyfayalite* such as (4) should have occurred during the temperature quench.

(2) it could result from a nucleation and growth process as described by Champness (1970). This would explain the crenels texture observed at the interface between the *fayalite* and the *laihunite* zones. This would also imply that longer exposure of the samples to the P-T-fO_2 conditions at which these zones grew may result in the formation of well-formed crystals of *laihunite*, *oxides* and *quartz*. The specific orientation of the lamellae would then probably be related to the kinetics and diffusion process of the defects in fayalite during oxidation. Defect diffusion is indeed faster in the c-direction than in the a-direction (Ullrich and Becker 2001).

In both cases, the existence of the *laihunite* phase – with the same composition of the *laihunite* zone – in nature (Shen et al. 1986) strongly hints at the stability of an "*oxyfayalite*" phase $Fe^{2+}_{0.26}Fe^{3+}_{1.16}\square_{0.58}SiO_4$ at some natural conditions that still must be determined.

Evolution of temperature, oxidation conditions and gas composition

The presence of three successive and distinct *fayalite* oxidation zones probably results from variations of the gas composition at near atmospheric pressure that occurred after the rhyolite flow emplacement. The formation of *fayalite* implies that the initial fO_2 in the lithophysae was below the *fayalite-magnetite-quartz* FMQ ($3\ Fe_2SiO_4 + O_2 = 2\ Fe_3O_4 + 3\ SiO_2$) buffer. The oxidation process certainly occurred by steps and the highest fO_2 value produced *hematite* (Fig.7). The presence of this *hematite* zone suggests that conditions above the *magnetite-hematite* MH ($4\ Fe_3O_4 + O_2 = 6\ Fe_2O_3$) buffer were reached. Pre-eruptive temperatures for rhyolite magmas vary between 650 and 1000°C (Carmichael et al. 1974; Honjo et al. 1992). Using geothermometry on Fe-Ti oxides, Castro et al. (2013) determined a pre-eruptive temperature of 870-920°C for the magma that feeds the Cordón Caulle eruption in Chile, the only currently erupting obsidian flow. *Tridymite*, which is present in Obsidian Cliffs' lithophysae, is known to form above 870°C at 1 atmosphere, although it has been proposed that this mineral can crystallize outside its stability field in a metastable form. Richnow (1999), for example, found slightly lower temperatures (~815°C) for the *tridymite*-bearing rhyolites of the Ngongotaha Dome, New Zealand. Obsidian Cliffs lava flow does not contain any phenocryst, indicating that the magma erupted at superliquidus temperature. Using the whole composition of the Obsidian Cliffs lava flow (76.5 ± 0.2 wt% SiO_2, 0.12 ± 0.01 wt% TiO_2, 13.1 ± 0.2 wt% Al_2O_3, 1.03 ± 0.03 wt% FeO_{total}, 0.04 ± 0.01 wt% MnO, 0.14 ± 0.03 MgO, 0.88 ± 0.03 wt% CaO, 4.2 ± 0.2

386 wt% Na_2O, 3.45 ± 0.06 wt% K_2O, 0.10 ± 0.01 wt% P_2O_5; Hildreth et al. 2012), we have
387 determined its potential liquidus temperature using MELTS (Ghiorso and Sack 1995). With 0.36
388 wt% H_2O (LOI, Hildreth et al. 2012), T liquidus would be ~1009°C. In fact, it is highly probable
389 that some gas was lost, and therefore, that the actual H_2O fraction was higher. Using the
390 maximum H_2O content of Newberry obsidian rocks (Rust et al. 2007), i.e. 1.34 wt%, $T_{liquidus}$ is
391 close to 944°C. Considering that the lithophysae-bearing parts of Obsidian Cliffs probably have
392 higher gas content, Obsidian Cliffs' rhyolite initial emplacement temperature is likely to be in
393 the 800-950°C range.

394 The oxidation occurred at near atmospheric pressure; therefore, the oxidation conditions
395 (log fO_2) during fayalite formation can be estimated below around -12.5 to -15 using the FMQ
396 buffer calculated by O'Neill (1987) (Fig.7). This range is concordant with the values found by
397 Richnow (1999) for the crystallization of Ngongotaha rhyolite using oxythermometry in the
398 groundmass (-13.43 to -14.30).

399 Water is the most likely gas species that occupied the vugs when they formed. However,
400 Deines (1974) determined that it should be at equilibrium with H_2 at 0.1 MPa and 900°C, for an
401 oxygen fugacity below the FMQ buffer. For a log fO2=-13.27 (FMQ-0.5), the gas should contain
402 H_2O and H_2 in the proportions 97:3 (mol%) and at log fO_2=-12.77. With constant gas
403 composition, fO_2 decreases parallel to FMQ with temperature (Fig.7). Fayalite oxidation can,
404 therefore, not be explained by simple cooling in a closed system. The formation of the different
405 oxidation layers could be explained in two ways:

406 (1) the loss of H_2 from the lithophysae. According to Zhang and Ni (2010), H_2 diffusion rate in
407 rhyolite is indeed ~50 times faster than the diffusion of H_2O, and ~3000 times faster than O_2.

(2) the infiltration of meteoric water into the lithophysae, which could also explain the partial destabilization of *osumilite* to *phlogopite.*

Other volatile elements, like C or S, could have also been present with H_2O in gas and influenced the fO_2 evolution during cooling (Lowenstern 2001, Gonnermann and Manga 2005). In the case of an H-O-C system, various species may have formed in the fluid phase depending on the pH (Garrels and Christ 1965; Holloway 1987). Iishi et al. (1997) investigated experimentally the oxidation of *fayalite* (Fa_{70} to Fa_{100}) in at 300 ± 5°C and 100 ± 10 bar in a gas composed of CO_2 + H_2. They determined that precipitates of *laihunite* plus *hematite* form in alkaline aqueous fluid after one week, and that *hematite* and amorphous *silica* form in acidic aqueous environments after one month. The temperature conditions in their experiments were, however, probably lower than in Obsidian Cliffs lithophysae during fayalite oxidation. Further experiments at various temperatures and C/H/O fractions would be necessary to determine if the exact paragenesis and texture of our samples can be reproduced. Sulfur might also have been present in the gas, as suggested by Clay et al (2012) for the Rocche Rosse obsidian flow. Martin et al. (2011) obtained compositions similar to Obsidian Cliffs' *laihunite* and "*oxyfayalite"* zones in experiments run at 1 GPa – 700-900°C using a carbon- and sulfur-rich silicate system without hydrogen. The resulting *laihunite* and *oxyfayalite* regions are heterogeneous as in Obsidians Cliffs' samples, but the amorphous SiO_2 appears either as lamellae or as rounded "inclusions". Further experiments are needed to reproduce the exact texture and composition of Obsidian Cliffs' fayalite oxidation products (work in progress). If hydrogen was present in the lithophysae, other gas species may also have formed, such as SO_2 or H_2S (Holloway 1977). To our knowledge, fayalite oxidation has not been studied in H-O-C-S-rich environments.

Kinetics of fayalite oxidation

Timescales of the *fayalite* crystals oxidation can be evaluated using experimental studies from the literature. Mackwell (1992) determined that *fayalite* oxidation at 770°C in air should produce an external oxide (*magnetite*) thickness of 7 ± 2 µm in 10 hours (which should grow to 15 ± 6 µm in 100 hours), and an internal two-phase oxide (*magnetite*) + *silica* layer thickness of 20 ± 5 µm (50 ± 20 µm after 100 hours). In Obsidian Cliffs' *fayalite*, internal oxidation layers are multiple, and the gas composition might be different. However, using his *fayalite* oxidation rates as a first approximation, the thickness of the internal oxidation layers (< 20 µm) indicates that the total oxidation process may have occurred in less than 10 hours, and was then interrupted by variations in the environmental conditions. The complex texture observed at the *fayalite* / *laihunite* interface confirms that the kinetics of the *fayalite* / gas interface influenced the equilibration of the system as well as diffusion processes in the bulk fayalite, as observed by Ullrich and Becker (2001). The kinetics of the *laihunite* / gas and "*oxyfayalite*" / gas interfaces also probably played a role that remains to be determined.

IMPLICATIONS

Insights on the structural evolution of *fayalite* with iron oxidation

In Obsidian Cliffs' rhyolite, *fayalite* oxidation was not continuous. Only some particular compositions are represented, corresponding to *fayalite* $Fe^{2+}_2SiO_4$, *laihunite* $Fe^{2+}Fe^{3+}_2\square(SiO_4)_2$ and "*oxyfayalite*" $Fe^{2+}_{0.26}Fe^{3+}_{1.16}\square_{0.58}SiO_4$. This suggests that there is no complete solid solution between *fayalite* and the theoretical pure "*ferrifayalite*" at the temperature – pressure – fO_2 conditions at which our samples were exposed. Considering our results and the studies on *laihunite* in other terrestrial or meteoritic samples, we conclude that the *laihunite* phase is

certainly stable only in a relatively small stability field. Similarly, "*oxyfayalite"* may form at some restricted T-P-fO_2 conditions, leading to five stable phases in the Fe^{2+}-Fe^{3+} mixing line: one end-member (*fayalite*) and four intermediate phases (*laihunite-2M, laihunite-3M/3Or, laihunite-1M* and "*oxyfayalite"*). With increasing Fe^{3+} content, the structure of *fayalite* also evolves. *Fayalite* orthorhombic structure (Pbmn) deforms to a monoclinic structure ($P2_1/b$) for the 66 % Fe^{3+}-bearing *laihunite* to be stable. Fe^{3+} is incorporated by the M2 site of *fayalite*, while vacancies □ are in the M1 site. The presence of 82 % Fe^{3+} in "*oxyfayalite*" would require that at least 0.16 atom p.f.u. Fe^{3+} is incorporated by the M1 site, producing 0.08 more vacancies in the structure. The reaction that would transform *laihunite* into an "*oxyfayalite*" mineral can be written:

$$0.24\ Fe^{2+}_{M1} + 0.06\ O_2 = 0.08\ \square + 0.16\ Fe^{3+}_{M1} + 0.04\ Fe^{3+}_2O_3 \quad (10)$$

This reaction would produce "free" *hematite,* in addition to "*oxyfayalite"*. It would also imply consequent deformation of the *fayalite* structure, which still has to be determined.

Role of degassing, meteoric infiltration and diffusion on *fayalite* oxidation processes

The rarity of the *laihunite* phase and the fact the "*oxyfayalite*" phase has never been observed could be explained by the variability of conditions during *fayalite* oxidation in lava flows. In Obsidian Cliffs rhyolite flow, the formation of the lithophysae occurred around 800-950°C, at the beginning of the solidification process of the lava (Fig.8). *Fayalite* oxidation zones analysis indicates that the gas composition in the lithophysae evolved during cooling. The mobility of the fluids is, therefore, a critical parameter. Two processes may be involved:

(1) the diffusion of volatiles in the rhyolite. The exsolution of gas from the magma is the source of the primary volatile species that filled the lithophysae. It occurred at high temperature through the nucleation and growth of bubbles simultaneous to or preceding the matrix

crystallization. Water was probably the first abundant species in the bubbles, although carbon and sulfur might also have exsolved early. Volatile diffusion from the lithophysae to the matrix upon the temperature decrease might also have promoted fayalite oxidation. In particular, H_2 is known to diffuse fast in rhyolite; its loss could have promoted a fO_2 increase and oxidized fayalite. The diffusion rates of the non-volatile elements also controlled the process of *fayalite* oxidation and the nature of the produced phases. Because of their various ionic radius, diffusion rates of Fe^{2+}, Fe^{3+}, Mg^{2+}, Mn^{2+}, Mn^{3+}, Si^{4+} and O^{2-} are different. Our data confirm that Mg^{2+} and Mn^{2+} diffuse faster than Fe^{2+} during fayalite oxidation process and were both soluble in the gas phase, leading to Mg- and Mn- free *laihunite* and "*oxyfayalite*" (see 4.2.1.).

(2) the infiltration of meteoric water, which probably occurred after the solidification of the lava flow (Anovitz et al. 2006), i.e. at relatively lower temperature. This infiltration could have created the fO_2 gradient at the crystal edges that resulted in the oxidation layer. No microfracturation is apparent in our sample; however, the presence of columnar jointing and of a large talus of debris at the lava flow edges is evidence for rock macrofracturation. Such macrofractures could have allowed meteoric water to infiltrate the lava flow to the depths of the lithophysae formation. The interconnection between the lithophysae (Fig.1c) could also have promoted water infiltration and *fayalite* oxidation.

ACKNOWLEDGMENTS

The authors thank D. Howard for providing some of the Obsidian Cliffs rhyolites samples. The authors gratefully acknowledge Yann Morizet, Jonathan Castro and an anonymous reviewer for their insightful and constructive comments. This research was supported by an appointment to

the NASA Postdoctoral Program at the Johnson Space Center, administered by Oak Ridge Associated Universities through a contract with NASA.

REFERENCES

Anovitz, L.M., Riciputi, L.R., Cole, D.R., Fayek, M., and Elam, J.M. (2006) Obsidian hydration: a new paleothermometer. Geology, 34, 517-520.

Ashworth, J.R., and Chambers, A.D. (2000) Symplectic reaction in olivine and the controls of intergrowth spacing in symplectites. Journal of Petrology, 41 (2), 285-304.

Blake, R.L., Hessevick, R.E., and Finger L.W. (1966) Refinement of the hematite structure. American Mineralogist, 51, 123-129.

Breitkreuz, C. (2013) Spherulites and lithophysae – 200 years of investigation on high-temperature crystallization domains in silica-rich volcanic rocks. Bulletin of Volcanology, 75 (4), 1-16.

Burt, D.M., Sheridan, M.F., Bikun, J.V., and Christiansen, E.H. (1982) Topaz rhyolites – distribution, origin, and significance for exploration. Economic Geology, 77, 1818-1836.

Carlier, G., Lorand, J.-P., and Kienast, J.R. (1994) Magmatic osumilite in an ultrapotassic dyke, southern Peru: first occurrence. European Journal of Mineralogy, 6, 657-665.

Carmichael, I., Turner, F., and Verhoogen, J. (1974) Igneous petrology. McGraw-Hill, New York, p739.

Castro, J.M., Schipper, C.I., Mueller, S., Militzer, AS., Amigo, A., Parejas, C.S, and Jacob, D. (2013) Storage and eruption of near-liquidus rhyolite magma at Cordón Caulle, Chile. Bulletin of Volcanology, 75 (702), 1-17.

Champness, P.E. (1970) Nucleation and growth of iron oxides in olivines, $(Mg,Fe)_2SiO_4$.

517 Mineralogical Magazine, 37 (291), 790-800.

518 Chen, Y., and Brantley, S.L. (2000) Dissolution of forsteritic olivine at 65°C and 2 < pH < 5.
519 Chemical Geology, 165, 267-281.

520 Christiansen, E.H., Burt, D.M., Sheridian, M.F., and Wilson, R.T. (1983) The petrogenesis of topaz
521 rhyolites from the Western United States. Contributions to Mineralogy and Petrology, 83, 16-
522 30.

523 Clay, P.L., O'Driscoll, B.O., Gertisser, R., Busemann, H., Sherlock, S.C., and Kelley, S.P. (2012)
524 Textural characterization, major and volatile element quantification and Ar-Ar systematics of
525 spherulites in the Rocche Rosse obsidian flow, Lipari, Aeolian Islands: a temperature
526 continuum growth model. Contributions to Mineralogy and Petrology, 165 (2), 373-395.

527 Deines, P., Nafziger, R.H., Ulmer, G.C., and Woermann, E. (1974) Temperature – oxygen fugacity
528 tables for selected gas mixtures in the system C-H-O at one atmosphere total pressure.
529 Bulletin of the Earth and Mineral Sciences Experiment Station 88, The Pennsylvania State
530 University, 129 pages.

531 Dyar, M.D., Delaney, J.S., Sutton, S.R., and Schaefer, M.W. (1998) Fe^{3+} distribution in oxidized
532 olivine: A synchrotron micro-XANES study. American Mineralogist, 83, 1361-1365.

533 Elmi, C., Brigatti, M.F., Pasquali, L., Montecchi, M., Laurora, A., Malferrari, D., and Nannarone, S.
534 (2010) Crystal chemistry, surface morphology and X-ray photoelectron spectroscopy of Fe-
535 rich osumilite from Mt. Arci, Sardinia (Italy). Physics and Chemistry of Minerals, 37, 561-569.

536 Faure, F., Trolliard, G., Montel, J.-M., and Nicollet, C. (2001) Nano-petrographic investigation of
537 a mafic xenolith (maar de Beaunit, Massif Central, France). European Journal of Mineralogy,
538 13, 27-40.

539 Fialin, M., Wagner, C., Metrich, N., Humler, E., Galoisy, L., and Bezos, A. (2001) $Fe^{3+}/\Sigma Fe$ vs. Fe*Lα*
540 peak energy for minerals and glasses: Recent advances with the electron microprobe.
541 American Mineralogist, 86, 456-465.
542 Fialin, M., Bézos, A., Wagner, C., Magnien, V., and Humler, E. (2004) Quantitative electron
543 microprobe analysis of $Fe^{3+}/\sum Fe$: basic concepts and experimental protocol for glasses.
544 American Mineralogist, 89, 654-662.
545 Fries, C. Jr., Schaller, W.T., and Glass, J.J. (1942) Bixbyite and pseudobrookite from the tin-
546 bearing rhyolite of the black range, New Mexico. American Mineralogist, 27, 305-322.
547 Frost, B.R. (1991) Introduction to oxygen fugacity and its petrologic importance. In: Lindsley
548 D.H., editor. Oxide Minerals: Petrologic and Magnetic significance. Mineralogical Society of
549 America, Reviews in Mineralogy, 25, 1-9.
550 Frost, D.J., and Wood, B.J. (1997) Experimental measurements of the fugacity of CO_2 and
551 graphite/diamond stability from 35 to 77 kbar at 925 to 1650°C. Geochimica et
552 Cosmochimica Acta, 61 (8), 1565-1574.
553 Fu, P., Kong, Y., and Zhang, L. (1982) Domain twinning of laihunite and refinement of its crystal
554 structure. Chinese Journal of Geochemistry, 1, 115-133.
555 Garrels, R.M., and Christ, C.L. (1965) Solutions, minerals, and equilibria. Harper's Geoscience.
556 Series, Harper and Row, New York. 450 p.
557 Ghiorso, M.S., and Sack, R.O. (1995) Chemical mass transfer in magmatic processes IV. A revised
558 and internally consistent thermodynamic model for the interpretation and extrapolation of
559 liquid-solid equilibria in magmatic systems at elevated temperatures and pressures.
560 Contributions to Mineralogy and Petrology, 119, 197-212.

Gloter, A., Guyot, F., Martinez, I., and Colliex, C. (2000) Electron energy-loss spectroscopy of silicate perovskite-magnesiowüstite high-pressure assemblages. American Mineralogist, 85, 1452-1458.

Gonnermann, H.M., and Manga, M. (2005) Nonequilibrium magma degassing: results from modeling of the ca. 1340 A.D. eruption of Mono Craters, California. Earth and Planetary Science Letters, 238, 1-16.

Grapes, R., Thornton, J., and Howard, D. (1993) Vug minerals in rhyolites, Henderson's Quarry, Mount Ngongotaha. Geological Society of New Zealand Miscellaneous Publications, 79A, 76.

Gualtieri A.F., Gemmi M. and Dapiaggi M. (2003) Phase transformations and reaction kinetics during the temperature-induced oxidation of natural olivine. American Mineralogist, 88, 1560-1574.

Hildreth, W., Fierstein, J., and Calvert, A.T. (2012) Geological map of the Three Sisters volcanic cluster, Cascades Range, Oregon. USGS Scientific Investigations Map 3186.

Holloway, J.R. (1977) Fugacity and activity of molecular species in supercritical fluids. Thermodynamics in Geology NATO Advanced Study Institutes Series 30, 161-181.

Holloway, J.R. (1987) Igneous fluids. Reviews in Mineralogy, 17, 211-233.

Honjo, N., Bonnichsen, B., Leeman, W.P., and Stormer, J.C., Jr. (1992) Mineralogy and geothermometry of high-temperature rhyolite from the central and western Snake River Plain. Bulletin of Volcanology, 54, 220-237.

Hua, X., and Buseck, P.R. (1995) Fayalite in the Kaba and Mokoia carbonaceous chondrites. Geochimica et Cosmochimica Acta, 59, 3, 563-578.

Huebner, J.S. (1971) Buffering techniques for hydrostatic systems at elevated pressures. In G.C.

583 Ulmer, Ed., Research Techniques for High Pressure and High Temperature, p. 123-177.
584 Springer-Verlag, New York.
585 Hwang, S.-L., Yui, T.-F., Chu, H.-T., Shen, P., Iizuka, Y., Yang, H.-Y., Yang, J., and Xu, Z. (2008)
586 Hematite and magnetite precipitates in olivine from the Sulu peridotite: a result of
587 dehydrogenation-oxidation reaction of mantle olivine? American Mineralogist, 93, 1051-
588 1060.
589 Iishi, K., Torigoe, K., and Han, X.J. (1997) Oriented precipitate complexes in iron-rich olivines
590 produced experimentally in aqueous oxidizing environment. Physics and Chemistry of
591 Minerals, 25 (1), 8-14.
592 Janney, D.E., and Banfield, J.F. (1998) Distribution of cations and vacancies and the structure of
593 defects in oxidized intermediate olivine by atomic-resolution TEM and image simulation.
594 American Mineralogist, 83, 799-810.
595 Jogo, K., Nakumura, T., Noguchi, T., and Zolotov, M.Y. (2009) Fayalite in the Vigarano CV3
596 carbonaceous chondrite: Occurrences, formation age and conditions. Earth and Planetary
597 Science Letters, 287, 320-328.
598 Khisina, N.R., Khramov, D.A., Kolosov, M.V., Kleshev, A.A., and Taylor, L.A. (1995) Formation of
599 ferriolivine and magnesioferrite from Mg-Fe olivine: reactions and kinetics of oxidation.
600 Physics and Chemistry of Minerals, 22 (4), 241-250.
601 Khisina, N.R., Khramov, D.A., Kleshev, A.A., and Langer, K. (1998) Laihunitization as a
602 mechanism of olivine oxidation. European Journal of Mineralogy, 10 (2), 229-238.
603 Khisina, N.R., Langer, K., Andrut, M., Ukhanov, V., and Wirth, R. (2000) Nano-scale
604 microstructure of Fe^{3+}-, OH^{-}-bearing-crystalline inclusions in experimentally oxidized olivine

605 from a mantle nodule. Mineralogical Magazine, 64 (2), 319-335.

606 Kitamura, M., Shen, B., Banno, S., and Morimoto, N. (1984) Fine textures of laihunite, a
607 nonstoichiometric distorted olivine-type mineral. American Mineralogist, 69, 154-160.

608 Kondoh, S., Kitamura, M., and Morimoto, N. (1985) Synthetic laihunite ($_{x}Fe^{2+}_{2-3x}Fe^{3+}_{2x}SiO_4$), an
609 oxidation product of olivine. American Mineralogist, 70, 737-746.

610 Kuebler, K.E. (2013) A combine electron microprobe (EMP) and Raman spectroscopic study of
611 the alteration products in Martian meteorite MIL 03346. Journal of Geophysical Research:
612 Planets, 118, 347-368.

613 Laihunite Research Group, Guiyang Institute of Geochemistry, Academia Sinica and Geological
614 Team 101, Liaoning Metallurgical and Geological Prospecting Company (1976) Geochemica,
615 2, 95-103 (in Chinese with English abstract).

616 Laihunite Research Group, Guiyang Institute of Geochemistry, Academia Sinica and Geological
617 Team 101, Liaoning Metallurgical and Geological Prospecting Company (1982) Chinese
618 Journal of Geochemistry, 1 (1), 105-115.

619 Lofgren, G. (1971a) Spherulitic textures in glassy and crystalline rocks. Journal of Geophysical
620 Research, 76, 5635-5648.

621 Lofgren, G. (1971b) Experimentally produced devitrification textures in natural rhyolitic glass.
622 Geological Society of America Bulletin, 82, 111-124.

623 Lowenstern, J.B. (2001) Carbon dioxide in magmas and implications for hydrothermal systems.
624 Mineralium Deposita, 36, 490-502.

625 Mackwell, S.J. (1992) Oxidation kinetics of fayalite (Fe_2SiO_4). Physics and Chemistry of Minerals,
626 19, 220-228.

627 Martin, A.M., Righter, K., Keller, L.P., Medard, E., Devouard, B., and Rahman, Z. (2011) Fayalite
628 oxidation processes: experimental evidence for the stability of pure ferric fayalite? 42nd Lunar
629 and Planetary Science Conference, The Woodlands. Abstract #2716.
630 Motoyoshi, Y., Hensen, B.S., and Arima, M. (1993) Experimental study of the high-pressure
631 stability limit of osumilite in the system K_2O-MgO-Al_2O_3-SiO_2: implication for high-
632 temperature granulite. European Journal of Mineralogy, 5, 439-445.
633 Muan, A., and Somiya, S. (1961) Stability relations of iron and manganese minerals: phase
634 equilibria at liquidus temperatures in the system iron oxide-manganese oxide-silica in air.
635 American Mineralogist, 46, 364-378.
636 Noguchi, T., Nakamura, T., Misawa, K., Imae, N., Aoki, T., and Toh, S. (2009) Laihunite and
637 jarosite in the Yamato 00 nakhlites: alteration products on Mars? Journal of Geophysical
638 Research, 114, E10004, doi:10.1029/2009JE003364.
639 Olesch, M., and Seifert, F. (1981) The restricted stability of osumilite under hydrous conditions
640 in the system K_2O-MgO-Al_2O_3-SiO_2-H_2O. Contributions to Mineralogy and Petrology, 76 (3),
641 362-367.
642 Olsen, E., and Bunch, T.E. (1970) Compositions of natural osumilites. American Mineralogist, 55,
643 875-879.
644 O'Neill, H.S.C. (1987) Quartz-fayalite-iron and quartz-fayalite-magnetite equilibria and the free
645 energy of formation of fayalite (Fe_2SiO_4) and magnetite (Fe_3O_4). American Mineralogist, 72,
646 67-75.
647 O'Neill, H.S.C. (1988) Systems Fe-O and Cu-O: Thermodynamic data for the equilibria Fe-"FeO",
648 Fe-Fe_3O_4, "FeO"-Fe_3O_4, Fe_3O_4-Fe_2O_3, Cu-Cu_2O and Cu_2O-CuO from emf measurements.

American Mineralogist, 73, 470-486.

O'Neill, H.S.C., and Pownceby, M.I. (1993) Thermodynamic data from redox reactions at high temperatures. II. The MnO – Mn_3O_4 oxygen buffer, and implications for the thermodynamic properties of MnO and Mn_3O_4. Contributions to Mineralogy and Petrology, 114, 315-320.

Pingqiu, F., Youhua, K., and Liu, Z. (1982) Domain twinning of laihunite and refinement of its crystal structure. Chinese Journal of Geochemistry, 1 (1), 115-133.

Richnow, J. (1999) Eruptional and post-eruptional processes in rhyolite domes. PhD thesis, University of Canterbury.

Rust, A.C., and Cashman, K.V. (2007) Multiple origins of obsidian pyroclasts and implications for changes in the dynamics of the 1300 B.P. eruption of Newberry Volcano, USA. Bulletin of Volcanology, 69 (8), 825-845.

Schaefer, M.W. (1983a) Measurements of iron(III)-rich fayalites. Nature, 303, 325-327.

Schaefer, M.W. (1983b) Crystal chemistry of ferric-rich fayalites. PhD thesis, Massachusetts Institute of Technology, Cambridge, Massachusetts.

Schaefer, M.W. (1985) Site occupancy and two-phase character of ferrifayalite. American Mineralogist, 71, 1455-1460.

Shen, B., Tamada, O., Kitamura, M., and Morimoto, N. (1986) Superstructure of laihunite-*3M* ($_{0.40}Fe^{2+}{}_{0.80}Fe^{3+}{}_{0.80}SiO_4$). American Mineralogist, 71, 1455-1460.

Shengyuan, W. (1982) The stability of laihunite – a thermodynamic analysis. Chinese Journal of Geochemistry, 1 (2), 233-245.

Smyth, J.R. (1975) High temperature crystal chemistry of fayalite. American Mineralogist, 60, 1092-1097.

671 Sueno, S., Cameron, M., and Prewitt, C.T. (1976) Orthoferrosilite: High-temperature crystal
672 chemistry. American Mineralogist, 61, 38-53.
673 Sueno, S., Matsuura, S., and Prewitt, C.T. (1985) Fe-deficient olivine structure type minerals
674 from Colorado, U.S.A. and Japan. Mineralogical Journal, 12 (8), 376-392.
675 Tamada, O., Shen, B., and Morimoto, N. (1983) The crystal structure of laihunite
676 ($_{0.40}Fe^{2+}_{0.80}Fe^{3+}_{0.80}SiO_4$) – nonstoichiometric olivine-type mineral. Mineralogical Journal, 11,
677 382-391.
678 Tomioka, N., Morlok, A., Koike, C., Köhler, M., and Grady, M. (2012) Laihunite in planetary
679 materials: An FTIR and TEM study of oxidized synthetic and meteoritic Fe-rich olivine. Journal
680 of Mineralogical and Petrological Sciences, 107, 157-166.
681 Ullrich, K., and Becker, K.D. (2001) Kinetics and diffusion of defects in fayalite, Fe_2SiO_4. Solid
682 State Ionics, 141-142, 307-312.
683 van Aken, P.A., and Liebscher, B. (2002) Quantification of ferrous/ferric ratios in minerals: new
684 evaluation schemes of Fe L_{23} electron energy-loss near-edge spectra. Physics and Chemistry
685 of Minerals, 29, 188-200.
686 Wu, T., and Kohlsted, D.L. (1988) Rutherford backscattering spectroscopy study of $(Mg,Fe)_2SiO_4$.
687 Journal of American Ceramic Society, 71 (7), 540-545.
688 Xu, H., Shen, Z., Konishi, H., Fu, P., and Szlufarska, I. (2014) Crystal structures of laihunite and
689 intermediate phases between laihunite-1M and fayalite: Z-contrast imaging and ab initio
690 study. American Mineralogist, 99, 881-889.
691 Zhang, Y., and Ni, H (2010) Diffusion of H, C and O components in silicate melts. Reviews in
692 Mineralogy and Geochemistry, 72, 171-225.

693 **LIST OF FIGURE CAPTIONS**

694 **Figure 1.** Photos of Obsidian Cliffs rhyolite lava flow. (a) General view of the northern cliff and its
695 debris talus, taken from an andesite lava flow of the Collier Cone (foreground). (b) Picture of a
696 glassy obsidian rock observed at the summit of Obsidian Cliffs lava flow, containing white
697 spherulites and deformed pink microlite flow banding (lens cap diameter is 62 mm). (c) Photo of
698 a lithophysae-rich sample. (d) and (e) Close-up images of oxidized *fayalite* crystals oriented in
699 two different directions (©B.Lechner and ©S.Wolfsried, respectively) showing external *hematite*
700 layers (red). Black crystals in lithophysae are *osumilite*, flat brown-red crystals are oxidized
701 *phlogopite* and white crystals are *tridymite*.

702 **Figure 2.** Photos of the lithophysae after cutting and polishing. (a) is a back-scattered electron
703 image of a whole *fayalite* crystal showing contrast variations corresponding to various degrees
704 of oxidation. The image was taken after the removal of the FIB slice (bright mark, upper left). (b)
705 is a reflected light image of a small part of the crystal. The red line indicates the location of the
706 FIB slice. It covers part of the *fayalite* zone (dark grey matrix), a *laihunite* zone (middle grey
707 zoning) and an "*oxyfayalite"* zone ("oxyfa"; light grey core). Image (c) shows large euhedral
708 osumilite crystals (light grey) that grew on small crystals of tridymite (BSE). Black areas were
709 formerly filled with gas. The rhyolite devitrified matrix is also visible at the bottom of the
710 picture. (d) is a BSE image of a phlogopite crystal that has been oxidized to hematite (light grey
711 elongated crystals).

712 **Figure 3.** (a) Microprobe analyses (in wt% oxides) of the various oxidation zones observed in
713 Obsidian Cliffs' (OC) *fayalite* crystals compared to theoretical compositions of *fayalite* and
714 "*ferrifayalite"*. The composition of the various *laihunite* polytypes are indicated for comparison:

715 *laihunite-3M* is from Shen et al. (1986) and *laihunite-1M*, *-3Or* and *-2M* from Xu et al. (2014).
716 The compositional trend of a theoretical Fe^{2+}-Mg^{2+} exchange between *fayalite* and *forsterite*
717 end-members is also reported, which explains Obsidian Cliffs' *fayalite* composition. (b)
718 Fe^{3+}/FeO_{total} in *fayalite* and its various oxidation zones, determined by electron microprobe
719 analysis (EMPA) and electron energy loss spectroscopy (EELS). The shift between Obsidian Cliffs
720 compositions and the oxidation line of fayalite is due to the presence of small fractions of Mg
721 and Mn.

722 **Figure 4.** Transmission electron microscope images of the *fayalite*, *laihunite* and "*oxyfayalite"*
723 zones. (a) Photo of the slice after cutting and ionic thinning by Focused Ion Beam. Fayalite
724 orientation (b and c axis) are reported in the upper left. The blue arrows on the image indicate
725 the position of "feathers" (see text). (b) Close-up image of a "feather" at the *fayalite* (left) –
726 *laihunite* (right) boundary. (c) Detail of the interface between *fayalite* and *laihunite*, showing the
727 relationship between the *laihunite* zone lamellae and the *fayalite* network. (d) Photo of the
728 lamellae in the *laihunite* zone. (e) Image of the *laihunite* (left) – "*oxyfayalite*" (right) interface. (f)
729 Photo of the lamellae in the "*oxyfayalite*" zone.

730 **Figure 5.** Selected Area Electron Diffraction (SAED) patterns and corresponding modeling of (a)
731 & (d) the *fayalite* zone (zone axis [001], indexed using positional parameters at 900°C from
732 Smyth 1975), (b) & (e) the dark lamellae from the *laihunite* zone and (c) & (f) the dark lamellae
733 from the "*oxyfayalite*" zone.

734 **Figure 6a.** Variation of the Fe*Lα* peak position as a function of the Fe content (in wt%) in the
735 *fayalite*, *laihunite* and "*oxyfayalite*" zones, compared to pure Fe^{2+} and Fe^{3+} standards,
736 determined using electron microprobe.

737 **Figure 6b.** Electron energy loss spectra (EELS) of iron for the (a) *fayalite*, (b) *laihunite* and (c)
738 "*oxyfayalite"* zones. Only FeL_3 was used for Fe^{3+}/Fe^{2+} calculation considering the low height of
739 the FeL_2 peaks.

740 **Figure 7.** log(fO_2) vs. temperature diagram at 1 atmosphere showing the theoretical evolution of
741 the fO_2 at the *fayalite* crystal edges and in the crystal fractures during cooling if the gas in the
742 lithophysae was composed of 97 mol% H_2O and 3 mol% H_2. Fayalite stability field is delimited by
743 the *fayalite* – m*agnetite* – q*uartz* (FMQ, 3 $Fe_2SiO_4 + O_2 = 2\ Fe_3O_4 + 3\ SiO_2$) reaction (O'Neill
744 1987). H_2 may have diffused outside of the lithophysae, inducing fayalite oxidation. The
745 infiltration of meteoric water could also have increased the fO_2. The m*agnetite* – h*ematite* (MH,
746 $4\ Fe_3O_4 + O_2 = 6\ Fe_2O_3$) buffer (Huebner 1971) indicate the minimum conditions where the
747 *hematite* zone has formed. The "oxyfayalite" formation conditions should be located right below
748 the HM buffer. The CCO ($C + O_2 = CO_2$) buffer (Frost and Wood 1997) and the MnO – Mn_3O_4 (6
749 $MnO + O_2 = 2\ Mn_3O_4$) buffer (O'Neill and Pownceby 1993) are also reported for comparison.

750 **Figure 8.** (A) Schematic view of the formation and oxidation of *fayalite* in the lithophysae during
751 Obsidian Cliffs' rhyolite flow cooling with corresponding estimations of temperature. (1)
752 Rhyolite emplacement. (2) Exsolution and crystallization in the core of the lava flow. (3)
753 Crystallization of fayalite, tridymite and osumilite in the lithophysae. (4) *Fayalite* oxidation. The
754 height of the lithophysae-rich zone and the size of the lithophysae were exaggerated for clarity's
755 sake. (B) Schematic cartoon representing the oxidation process with time along a fluid-filled
756 fracture inside a *fayalite* crystal or at a *fayalite* crystal edge.

757

Figure 1

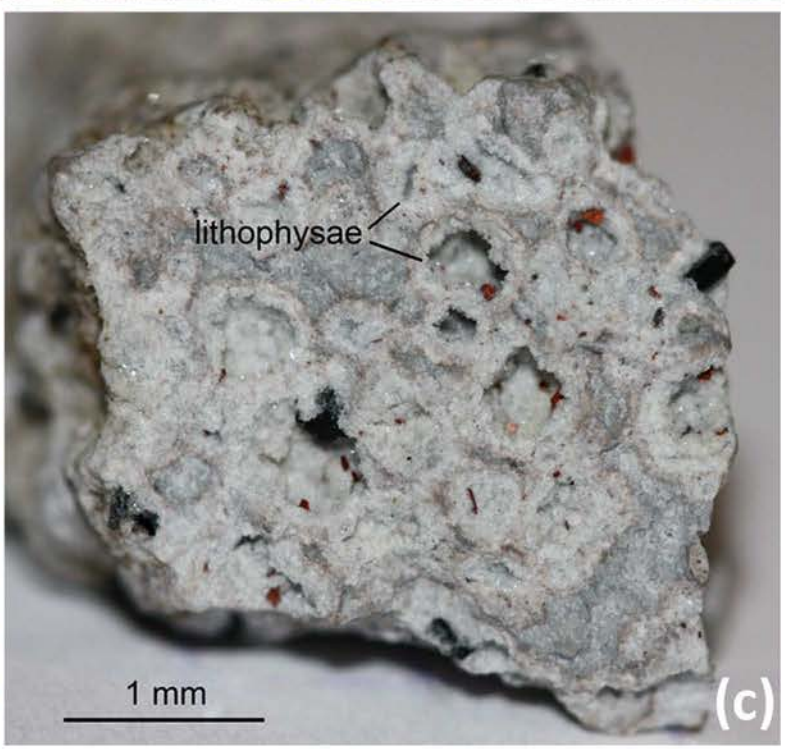

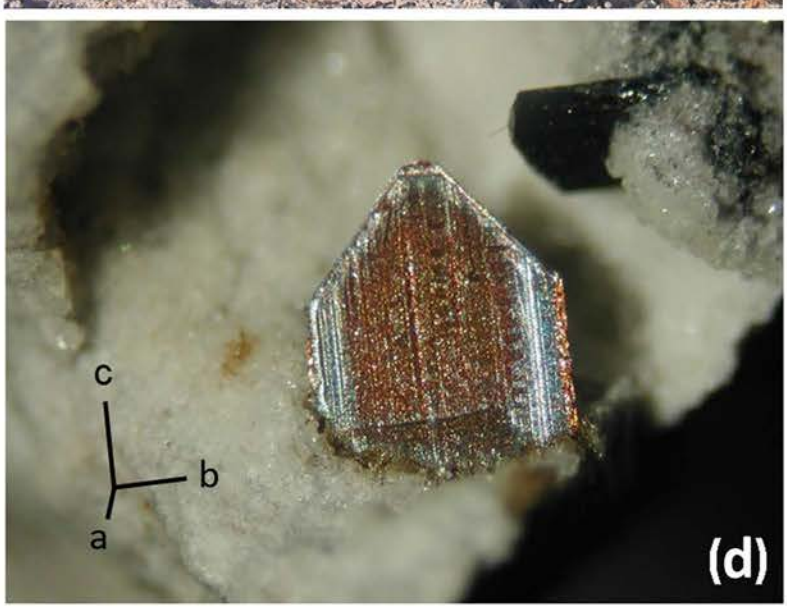

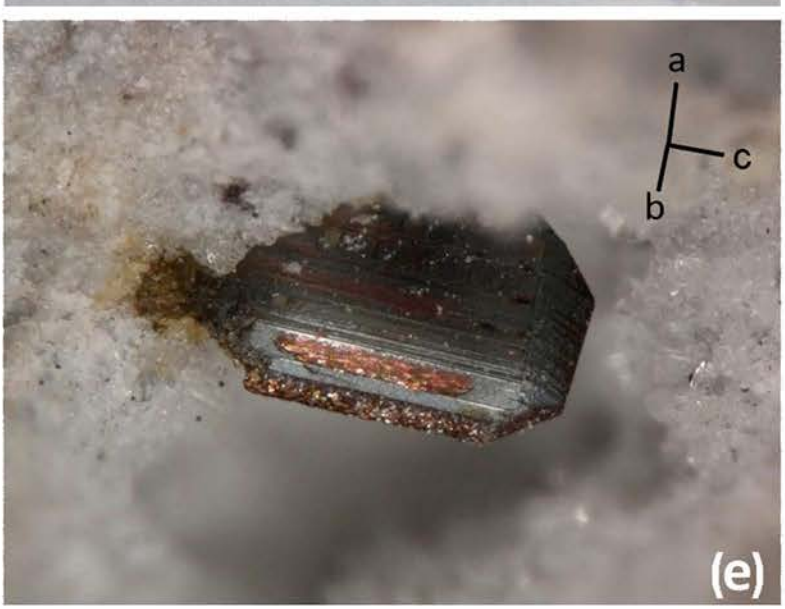

Figure 2

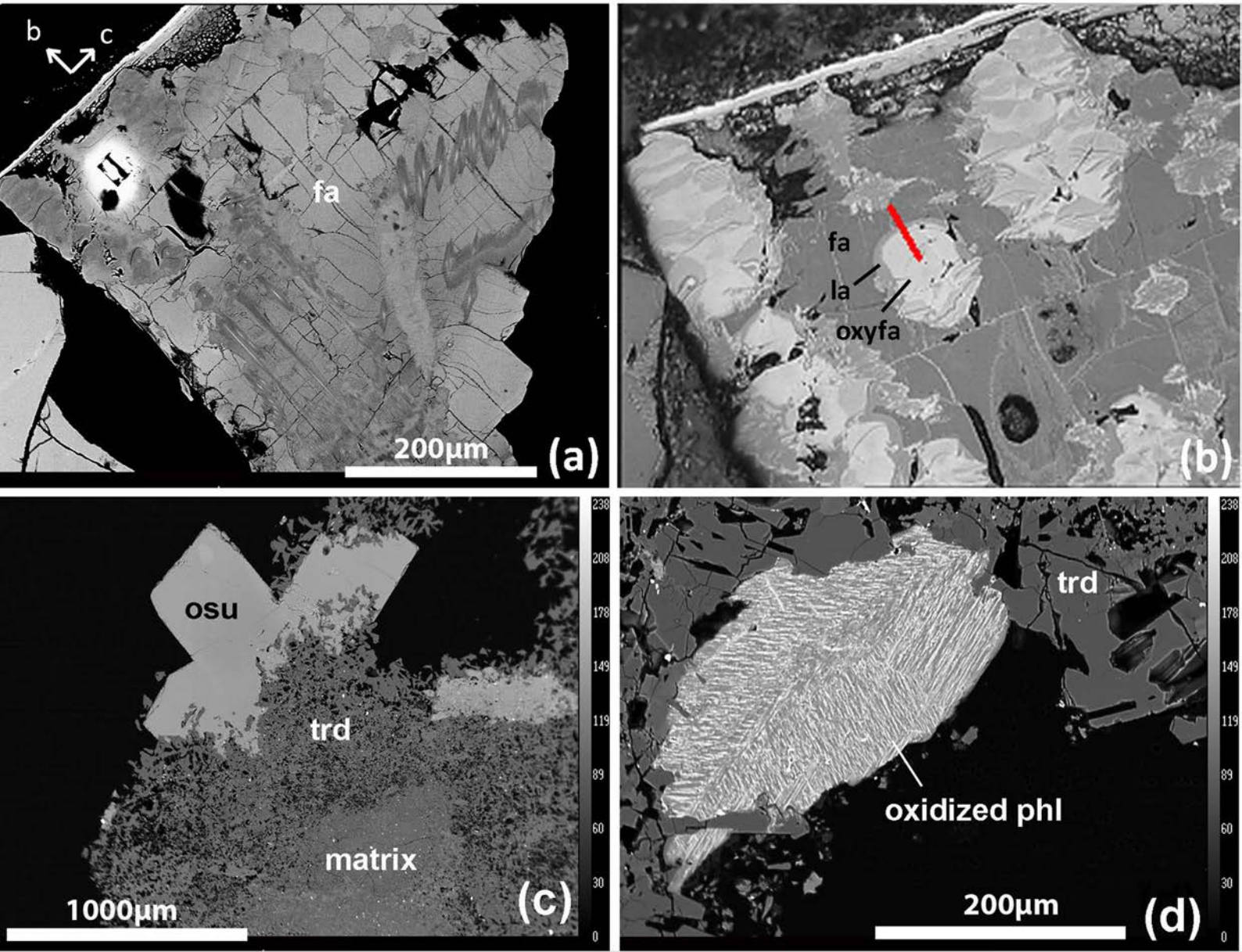
b
c
fa
200µm
(a)
fa
la
oxyfa
(b)
osu
trd
matrix
1000µm
(c)
238
208
178
149
119
89
60
30
0
trd
oxidized phl
200µm
(d)

Figure 3

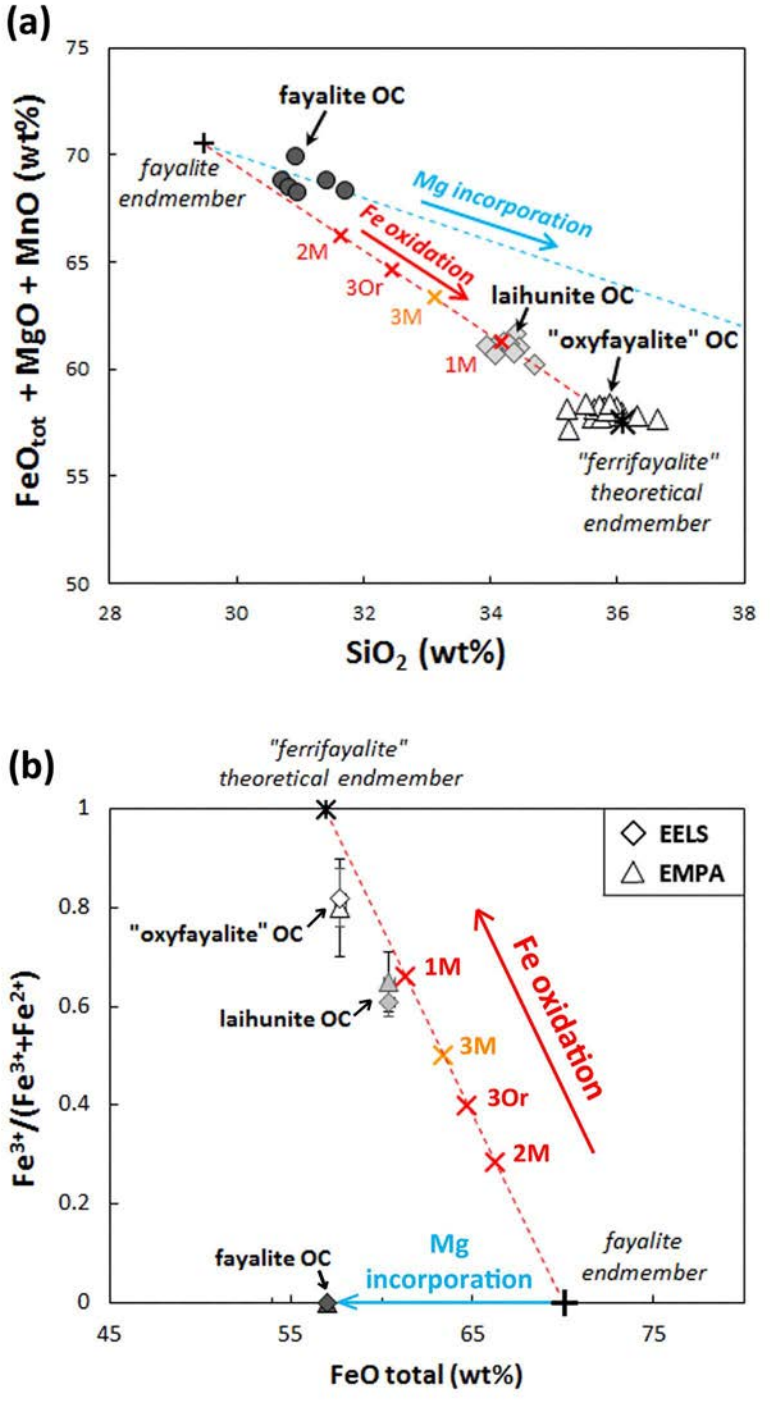
(a)
fayalite OC
fayalite endmember
Mg incorporation
Fe oxidation
2M
3Or
3M
laihunite OC
1M
"oxyfayalite" OC
"ferrifayalite" theoretical endmember
FeOtot + MgO + MnO (wt%)
SiO2 (wt%)
(b)
"ferrifayalite" theoretical endmember
EELS
EMPA
"oxyfayalite" OC
laihunite OC
1M
3M
3Or
2M
Fe oxidation
fayalite OC
Mg incorporation
fayalite endmember
Fe3+/(Fe3++Fe2+)
FeO total (wt%)

Figure 4

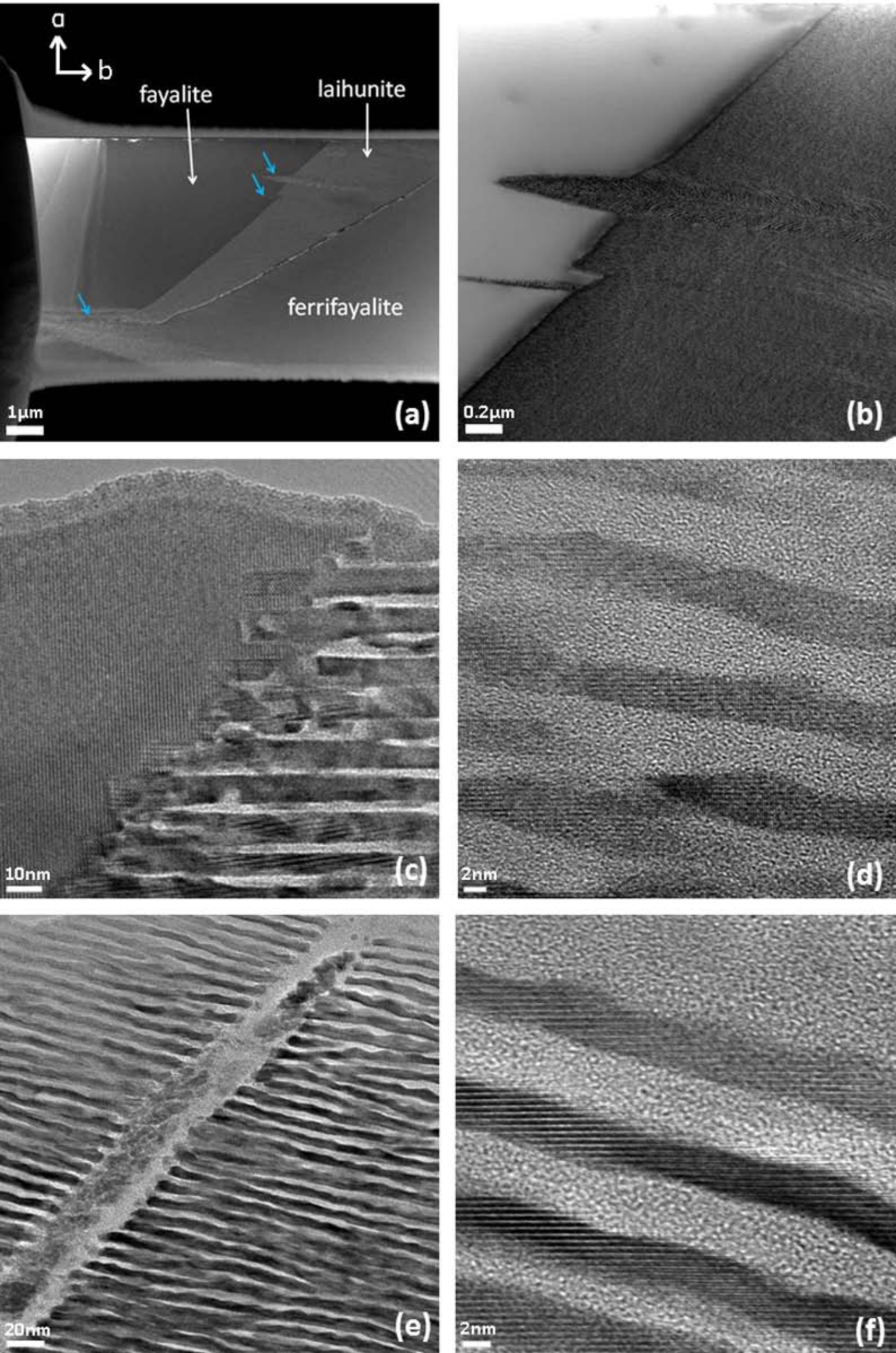
a
b
fayalite
laihunite
ferrifayalite
1μm
(a)
0.2μm
(b)
10nm
(c)
2nm
(d)
20nm
(e)
2nm
(f)

Figure 5

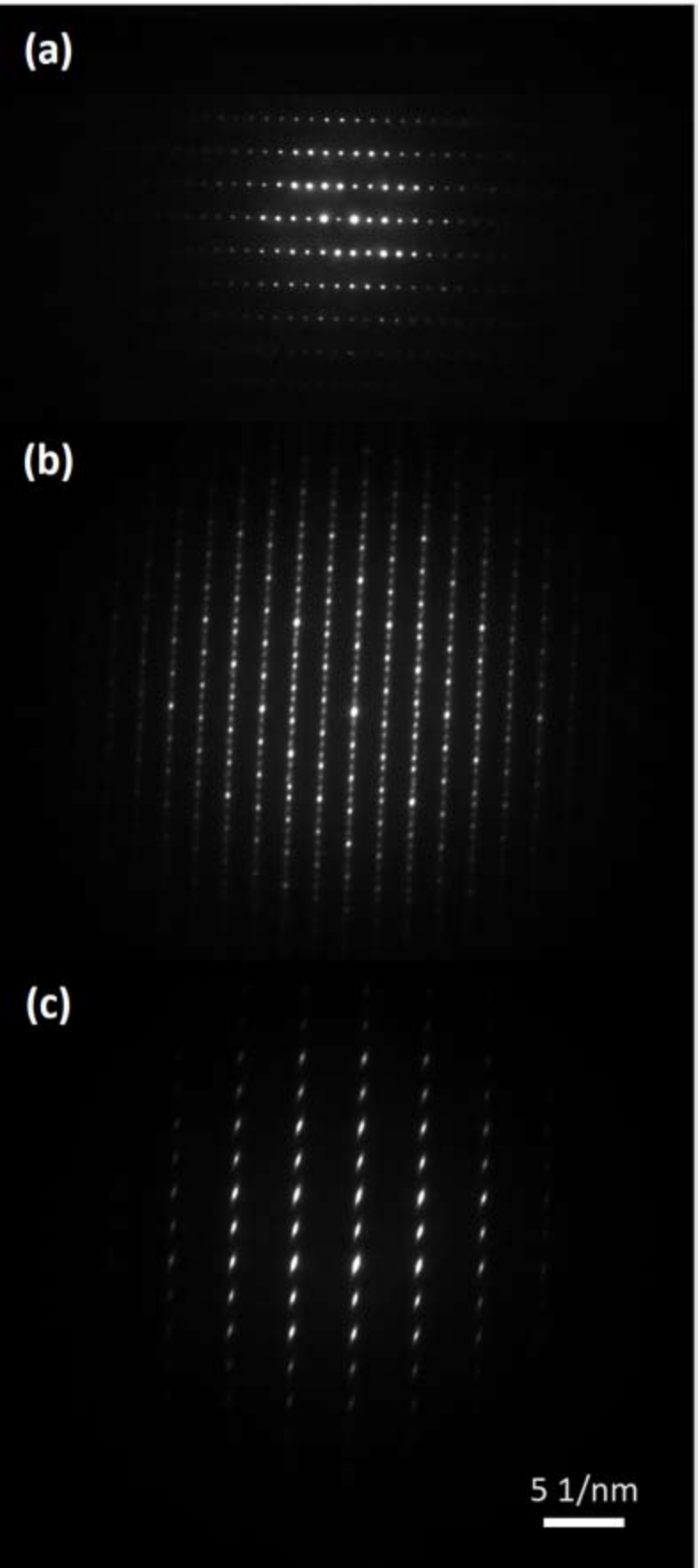
(a)
(b)
(c)
5 1/nm

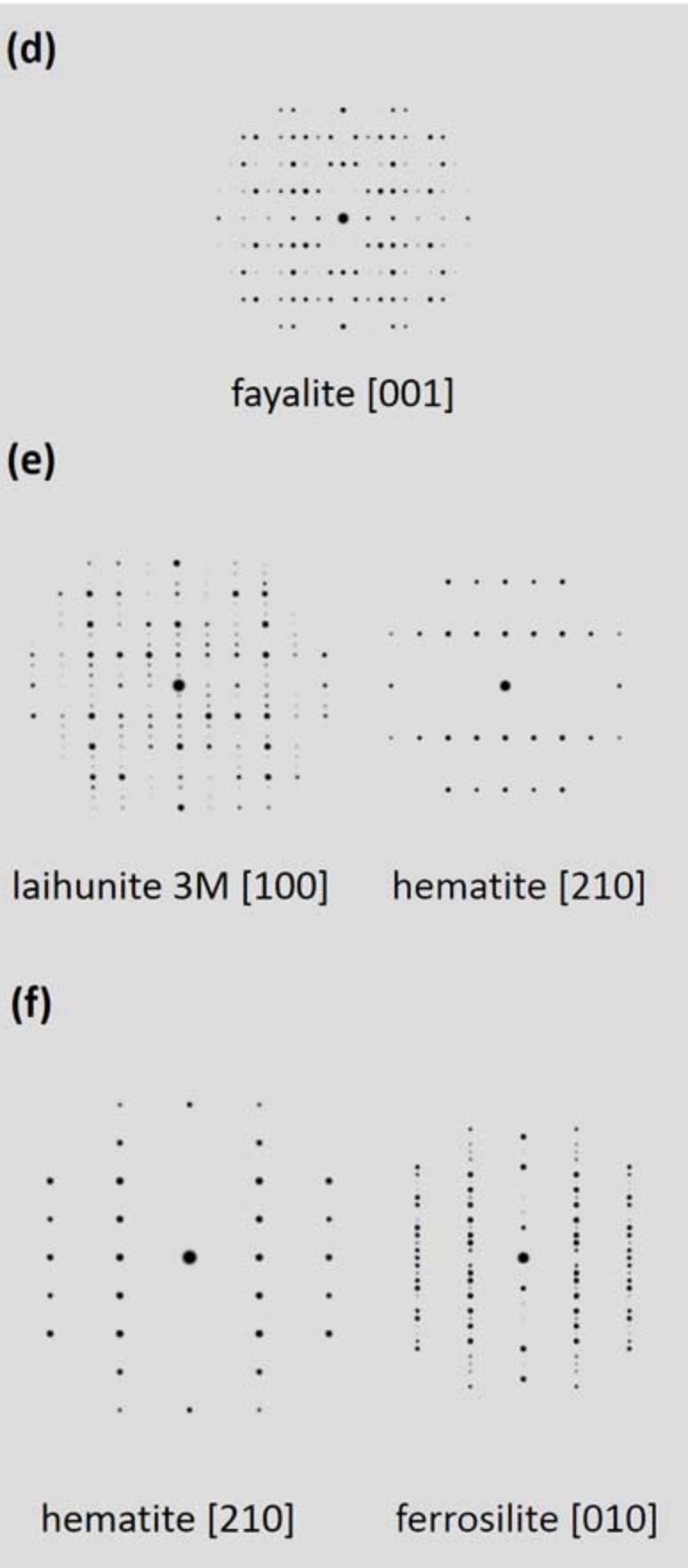
(d)
fayalite [001]
(e)
laihunite 3M [100]
hematite [210]
(f)
hematite [210]
ferrosilite [010]

Figure 6a

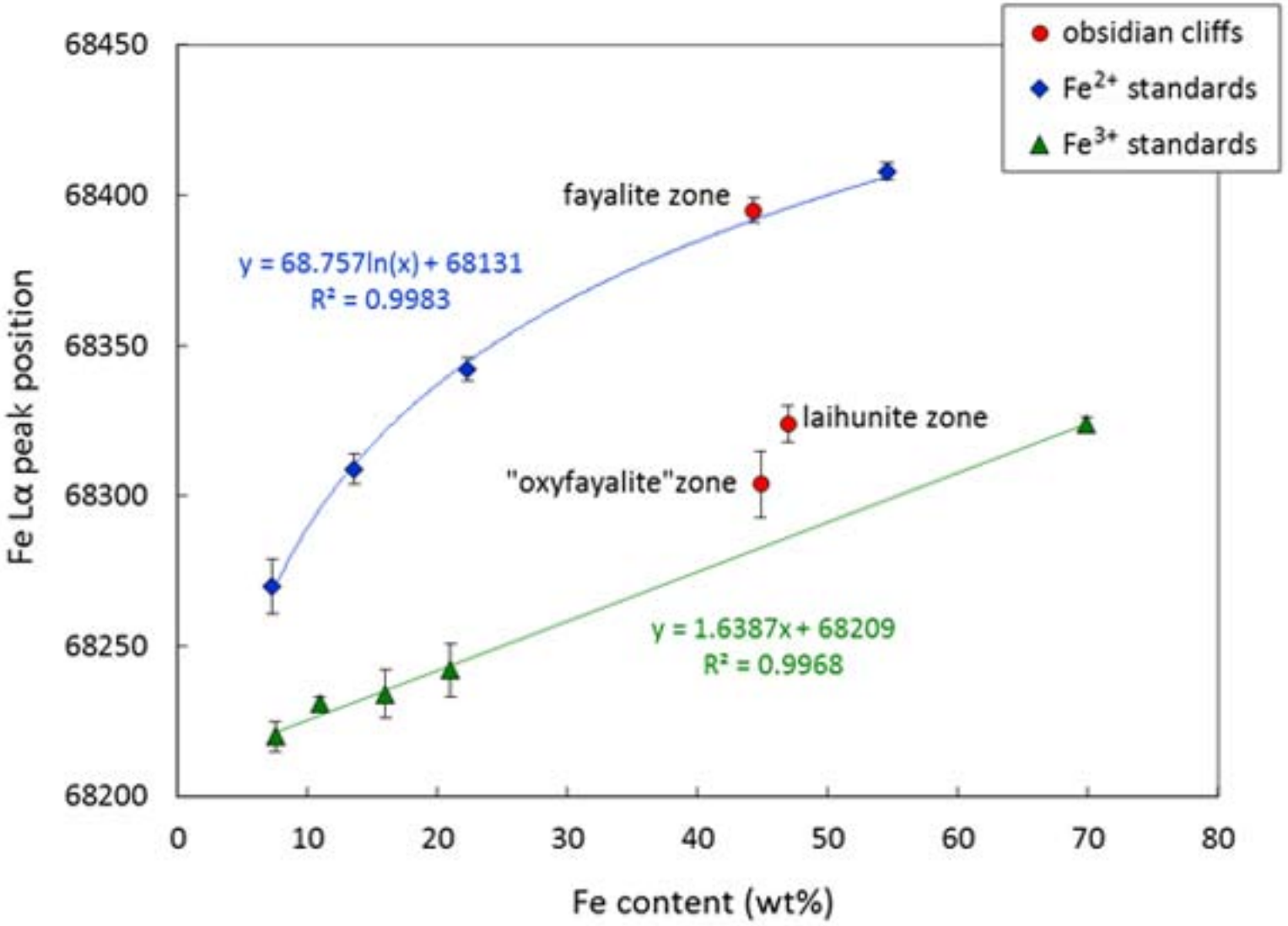
obsidian cliffs
Fe2+ standards
Fe3+ standards
fayalite zone
y = 68.757ln(x) + 68131
R² = 0.9983
laihunite zone
"oxyfayalite"zone
y = 1.6387x + 68209
R² = 0.9968
Fe Lα peak position
Fe content (wt%)
68450
68400
68350
68300
68250
68200
0
10
20
30
40
50
60
70
80

Figure 6b

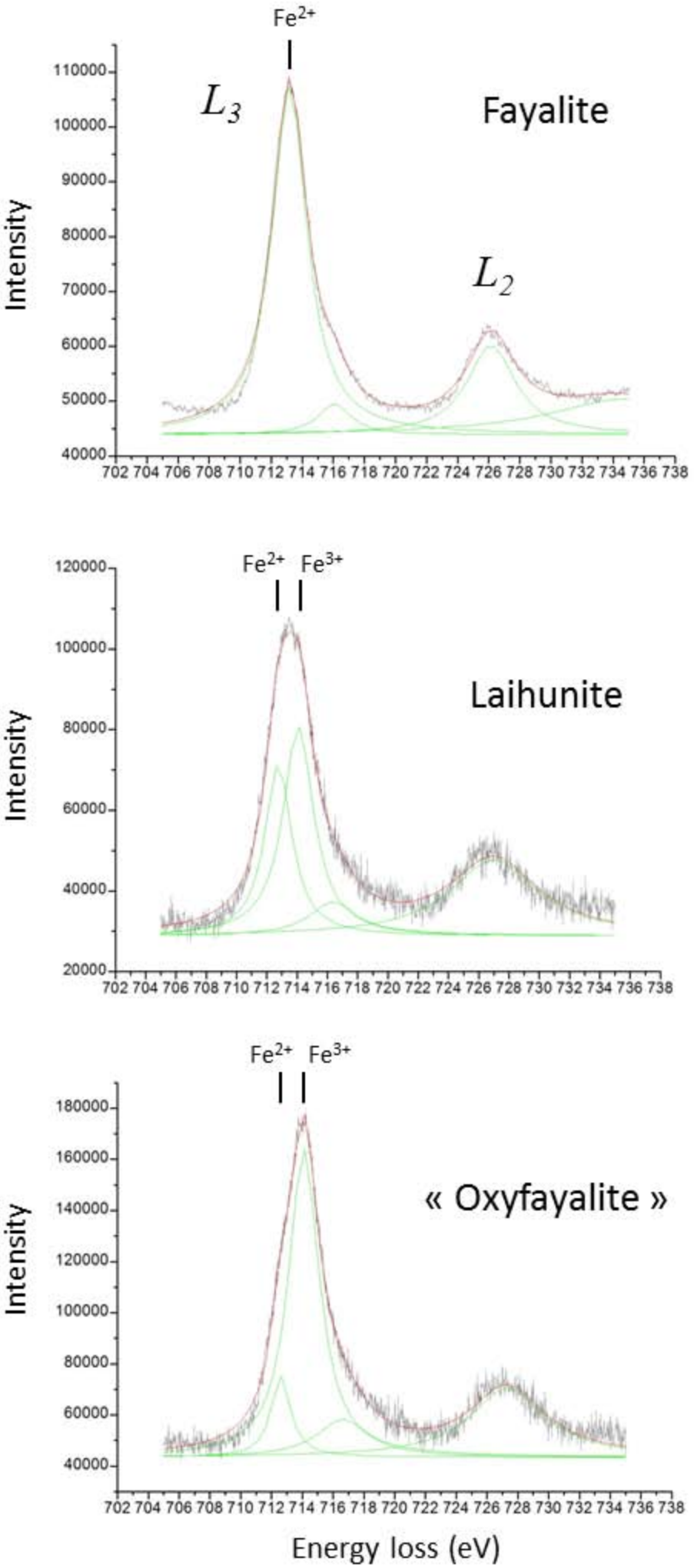
Fe2+
L3
L2
Fayalite
Intensity
110000
100000
90000
80000
70000
60000
50000
40000
702 704 706 708 710 712 714 716 718 720 722 724 726 728 730 732 734 736 738
Fe2+ Fe3+
Laihunite
120000
100000
80000
60000
40000
20000
« Oxyfayalite »
180000
160000
140000
120000
100000
80000
60000
40000
Energy loss (eV)

Figure 7

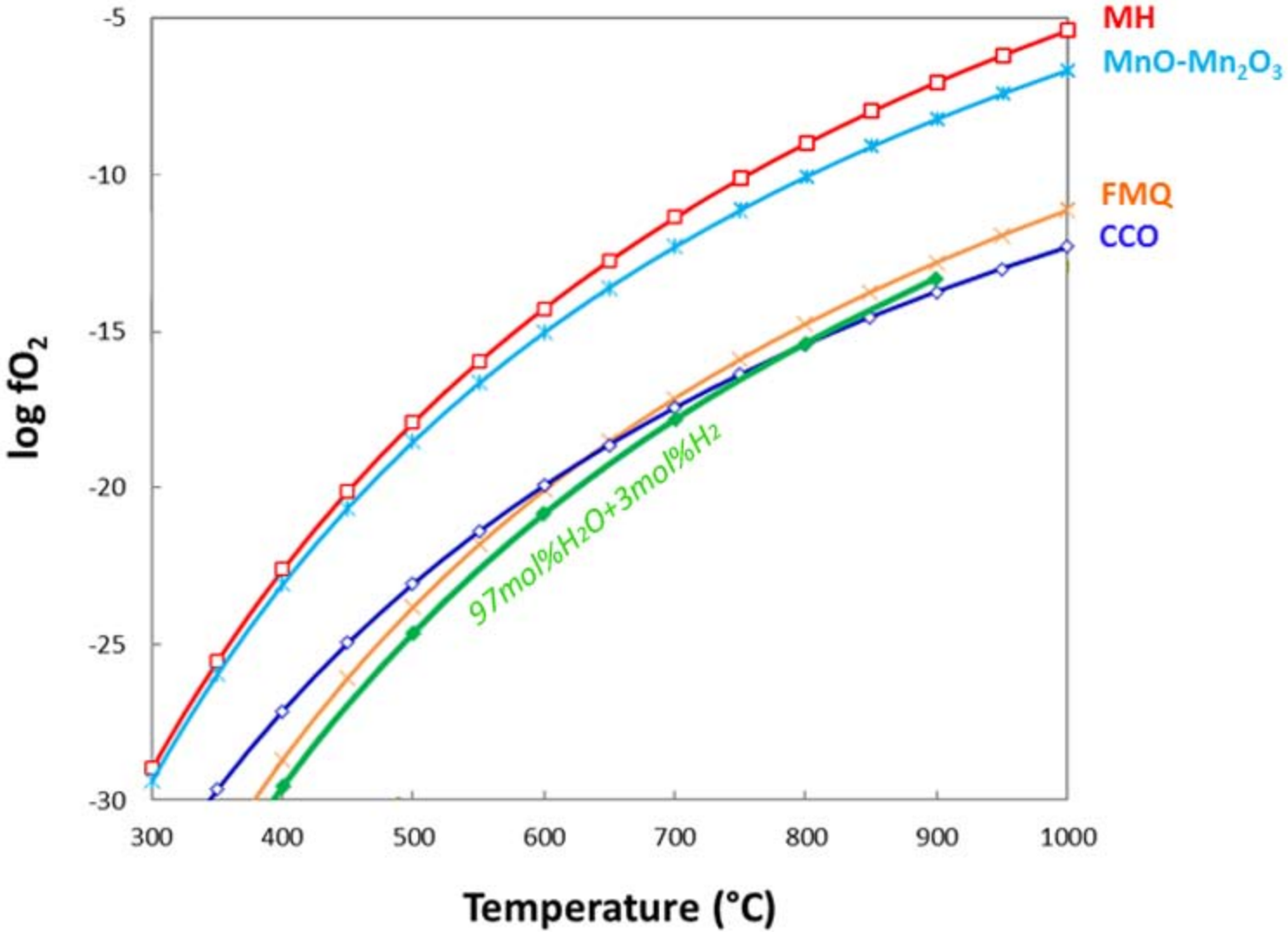
MH
MnO-Mn2O3
FMQ
CCO
97mol%H2O+3mol%H2
log fO2
-5
-10
-15
-20
-25
-30
300
400
500
600
700
800
900
1000
Temperature (°C)

Figure 8

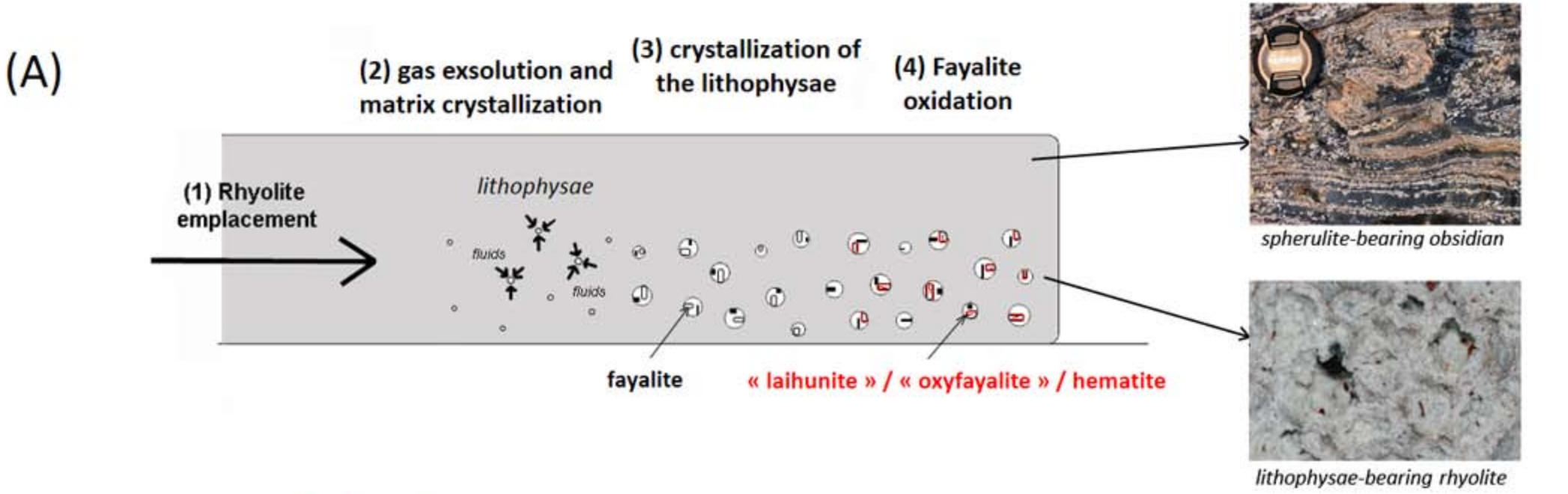
(A)
(2) gas exsolution and matrix crystallization
(3) crystallization of the lithophysae
(4) Fayalite oxidation
(1) Rhyolite emplacement
lithophysae
fluids
fluids
fayalite
« laihunite » / « oxyfayalite » / hematite
spherulite-bearing obsidian
lithophysae-bearing rhyolite
(B)
Fracture / Crystal Edge
a axis
fa
fluid
b axis
i Fayalite growth
nucleation and growth
fa
la
fluid
ii « Laihunite » zone formation
nucleation and growth?
dissolution?
fa
la
oxyfa
fluid
iii « Oxyfayalite » zone formation
fO_2
fa
la
oxyfa
hem
fluid
iv Hematite zone formation
~950-800°C
Cooling + Modification of the fluid composition (volatile diffusion, water infiltration)